

THESIS FOR THE DEGREE OF DOCTOR OF PHILOSOPHY IN NATURAL SCIENCE,
SPECIALIZING IN CHEMISTRY

From Silica Nano-Particles to Silica Gels and Beyond

Salt Induced Aggregation of Silica Nano-Particles and
the Stability of Resultant Gels

Christian Sögaard



UNIVERSITY OF GOTHENBURG

Department of Chemistry and Molecular Biology

Gothenburg, Sweden, 2020

From Silica Nano-Particles to Silica Gels and Beyond

Salt Induced Aggregation of Silica Nano-Particles and the Stability of Resultant Gels

Christian Sögaard

©Christian Sögaard

ISBN: 978-91-7833-906-8 (TRYCK)

ISBN: 978-91-7833-907-5 (PDF)

Department of Chemistry and Molecular Biology

University of Gothenburg

SE-41296 Gothenburg

Sweden

Telephone +46(0)31-786 00 00

Printed by Stema Specialtryck AB, Box 969, 501 10 Borås

“I’d rather be a rising ape than a falling angel.”

- Sir Terry Pratchett (1948 – 2015)

List of Papers

- Paper I: Silica sol as grouting material: A physio-chemical analysis
Christian Sögaard, Johan Funehag, Zareen Abbas
- Paper II: The specific co-ion effect on gelling and surface charging of silica nanoparticles: Speculation or reality?
Isabelle Simonsson, Christian Sögaard, Mark Rambaran, Zareen Abbas
- Paper III: Hofmeister effects in the gelling of silica nanoparticles in mixed salt solutions
Christian Sögaard, Krzysztof Kolman, Max Christensson, Ayşe Birsen Otyakmaz, Zareen Abbas
- Paper IV: Development and evaluation of polyether ether ketone (PEEK) capillary for electrospray
Christian Sögaard, Isabelle Simonsson, Zareen Abbas
- Paper V: Temperature and particle-size effects on the formation of silica gels from silica sols
Christian Sögaard, Magnus Hagström, Zareen Abbas
- Paper VI: The long term stability of silica nanoparticle gels in waters of different ionic compositions and pH values
Christian Sögaard, Johan Funehag, Marino Gergorić, Zareen Abbas

Contribution Report

Paper I: I conducted literature study and wrote most of the article

Paper II: I was involved in data analysis and wrote the MatLab script used for the titration results. I conducted gel time tests. I wrote part of the article.

Paper III: I was involved with planning and conducting gel time tests. I ran the molecular dynamics simulations but did not design the simulation system. I was heavily involved with the data analysis and wrote most of the paper.

Paper IV: I manufactured the PEEK capillaries. I ran the ES-SMPS tests and analysed the data. I wrote most of the article.

Paper V: I planned and performed the experiments, evaluated and was heavily involved in discussions around the results. I wrote the paper.

Paper VI: I was heavily involved in the design of the equipment and which waters and salts to test. I conducted the tests and was involved in the ICP-AES measurements. I wrote most of the article.

Abstract

Aqueous silica nanoparticle suspensions are widely available and used within a number of industries. A relatively new area of application is as a grouting material for sealing narrow fractures in tunnels. While silica sols/gels have been used successfully to grout sections of tunnels the continued reliability of the grouting requires knowledge of gel formation, long time stability and functionality. Although much research has been done for silica nanoparticle interactions with monovalent cations, the effect of anions and gelling in salt mixtures has not been thoroughly investigated. Ionic interactions with the silica surface were investigated by potentiometric titrations and gel time tests. The strength of cation interaction with the silica surface is found to be controlled by cation and anion interactions in bulk salt solution in the following order $\text{Cl}^- \approx \text{ClO}_4^- < \text{ClO}_3^- < \text{NO}_3^- < \text{SO}_4^-$. Anions to the left in the ranking lead to shorter gel times and higher surface charge density, indicating stronger cation-surface interactions. In salt mixtures with divalent and monovalent ions generally the cations interaction with silica surface follows the direct Hofmeister series. However, there are considerable differences seen in the kinetics of gel formation. Strongly interacting cations in a mixture of monovalent cations and divalent cations, determine the gelling kinetics. For divalent cations an unexpected shift in the Hofmeister series was observed for Mg^{2+} at $\text{pH} > 8$. It is expected that Mg^{2+} due to its strong hydration should follow the direct Hofmeister series as Li^+ does i.e., weakly interacting with silica surface due to strong hydration, than Ca^{2+} , but this is not the case. However, at $\text{pH} < 8$ the direct Hofmeister series was observed. The plausible explanation for this unusual strong interaction of Mg^{2+} with negatively charged silica surface compared to Ca^{2+} is its ability to polarize the hydrating water molecules leading to strong interaction with silica surface.

The effect of temperature and particle size on the aggregation behaviour is investigated using gel time tests, rheological measurements, and electrospray scanning mobility particle sizer. Smaller average particle size and increased temperature lead to faster aggregation due to increased Brownian motion causing higher number of particle collisions in the sols. The formation of a gel network is sudden, leading to an exponential increase in complex viscosity. The average number of particles contained in an aggregate of average size at the

gel point was found to be three, indicating that large numbers of particles are not incorporated in the gel network at the gel point.

To test the long-time stability of silica gels new test equipment was designed and constructed. Waters of different ionic composition and pH were pushed through gels and leachates were collected for maximum 488 days and were analysed by inductively coupled plasma atomic emission spectroscopy for metal concentrations. It was found that much of the salt such as NaCl used to generate the gels exits with the water. The amount of salt exiting follows the direct Hofmeister series for monovalent cations i.e., Na⁺ leaching more than K⁺. Increased pH of the water entering the gels does not lead to increased silica dissolution since the silica gels buffer the water down to pH \approx 9-10. Using a simple numerical method the collected data is used to predict the lifetime of the grouted silica gels. The lifetime is calculated to be between 200 and 400 years depending on different factors such as flow rate through the gels and salt used to form the gels.

Abstract in Swedish

Vattenhaltiga kiseldioxid-nanopartikelsuspensioner är allmänt tillgängliga och används inom ett antal industrier. Ett relativt nytt användningsområde är som ett injekterings-material för tätning av smala sprickor i tunnlår. Medan kiseldioxidpartiklar/geler har använts framgångsrikt för att injektera sektioner av tunnlår kräver fortlöpande tillförlitlighet av injekteringen kunskap om gelbildning, långvarig stabilitet och funktionalitet. Även om mycket forskning har gjorts för kiseldioxid-nanopartikel interaktioner med monovalenta katjoner, har effekten av anjoner och gelning i saltblandningar inte undersökts noggrant. Joniska interaktioner med kiseldioxidytan undersöktes med potentiometriska titrerings- och geltidstester. Styrkan för katjoninteraktion med kiseldioxidytan har visat sig kontrolleras av katjon- och anjoninteraktioner i bulk-saltlösning i följande ordning $\text{Cl}^- \approx \text{ClO}_4^- < \text{ClO}_3^- < \text{NO}_3^- < \text{SO}_4^-$. Anjoner till vänster i rankningen leder till kortare gel-tider och högre ytladdningsdensitet, vilket indikerar starkare katjon-ytinteraktioner. I saltblandningar med tvåvärda och envärda joner följer i allmänhet katjonernas interaktion med kiseldioxid den direkta Hofmeister-serien. Det finns emellertid avsevärda skillnader i gelbildningens kinetik. Starka växelverkande katjoner i en blandning av envärda katjoner och tvåvärda katjoner, bestämmer gelningskinetiken. För tvåvärda katjoner observerades en oväntad förändring i Hofmeister-serien för Mg^{2+} vid $\text{pH} > 8$. Det förväntas att Mg^{2+} på grund av dess starka hydrering bör följa den direkta Hofmeister-serien som Li^+ gör, d.v.s. svag samverkande med kiseldioxidytan på grund av starkare hydrering, än Ca^{2+} , men detta är inte fallet. Vid $\text{pH} < 8$ observerades emellertid den direkta Hofmeister-serien. Den troliga förklaringen till denna ovanliga starka interaktion mellan Mg^{2+} med den negativt laddade kiseldioxidytan jämfört med Ca^{2+} är dess förmåga att polarisera de hydratiserande vattenmolekylerna vilket leder till stark interaktion med kiseldioxidytan.

Effekten av temperatur och partikelstorlek på aggregeringsbeteendet undersöks med användning av geltidstester, reologiska mätningar och ES-SMPS mätningar. Mindre genomsnittlig partikelstorlek och ökad temperatur leder till snabbare aggregering på grund av ökad Brownian rörelse som orsakar högre antal partikelkollisioner i lösningarna. Bildningen av ett gelnät är plötslig, vilket leder till en exponentiell ökning av komplex viskositet. Det genomsnittliga antalet partiklar som ett aggregat av medelstorlek innehöll vid

gelpunkten befanns vara tre, vilket indikerar att ett stort antal partiklar inte är införlivade i gelnätverket vid gelpunkten. För att testa den långvariga stabiliteten hos kiseldioxidgeler, designades och konstruerades ny testutrustning. Vatten med olika jonisk sammansättning och pH pressades genom geler och lakvatten uppsamlades under maximalt 488 dagar och analyserades genom induktivt kopplad plasma - atomemissionsspektroskopi för metallkoncentrationer. Det visade sig att mycket av saltet, så som NaCl, som användes för att generera gelerna lämnade gelerna med vattnet. Mängden salt som lämnar följer den direkta Hofmeister-serien för monovalenta katjoner, d.v.s. Na^+ lakar mer än K^+ . Ökat pH hos vattnet som kommer in i gelerna leder inte till ökad kiseldioxidupplösning eftersom kiseldioxidgelerna buffrar vattnet ner till $\text{pH} \approx 9-10$. Med hjälp av en enkel numerisk metod används de insamlade uppgifterna för att förutsäga livslängden för kiseldioxidgelerna. Livslängden beräknas till mellan 200 och 400 år beroende på olika faktorer såsom flödes hastighet genom gelerna och salt som används för att bilda gelerna.

Contents

1. Introduction.....	1
1.2. Aim.....	3
2. Background.....	4
2.1 Nanomaterials	4
2.2. Silica sols.....	5
2.2.1. Production	5
2.2.2. Surface Chemistry and Stabilization.....	7
2.2.3. Interaction of silica surface and ions - Destabilization.....	13
2.3 Aggregation of silica sols – Gelling mechanics	16
2.4 Silica gels.....	17
3. Methods	19
3.1. Gel time tests.....	19
3.2. Potentiometric titration	20
3.3. Molecular dynamics simulations	21
3.4. Dynamic light scattering.....	22
3.5. Electropray scanning mobility particle sizer	24
3.6. Long term gel stability tests	29
3.6.1. Design of test equipment	29
3.6.2. Test setup	30
3.7. Inductively coupled plasma – atomic emission spectroscopy	32
4. Results and discussion.....	33
4.1. Ion-silica interaction.....	33
4.1.1. Co-ion effects	33
4.1.2 Divalent ions.....	36
4.1.3. Mixed salts.....	41
4.2. Long term gel stability tests	43
5. Conclusions and future work.....	55
6. Acknowledgements	58
7. References	59

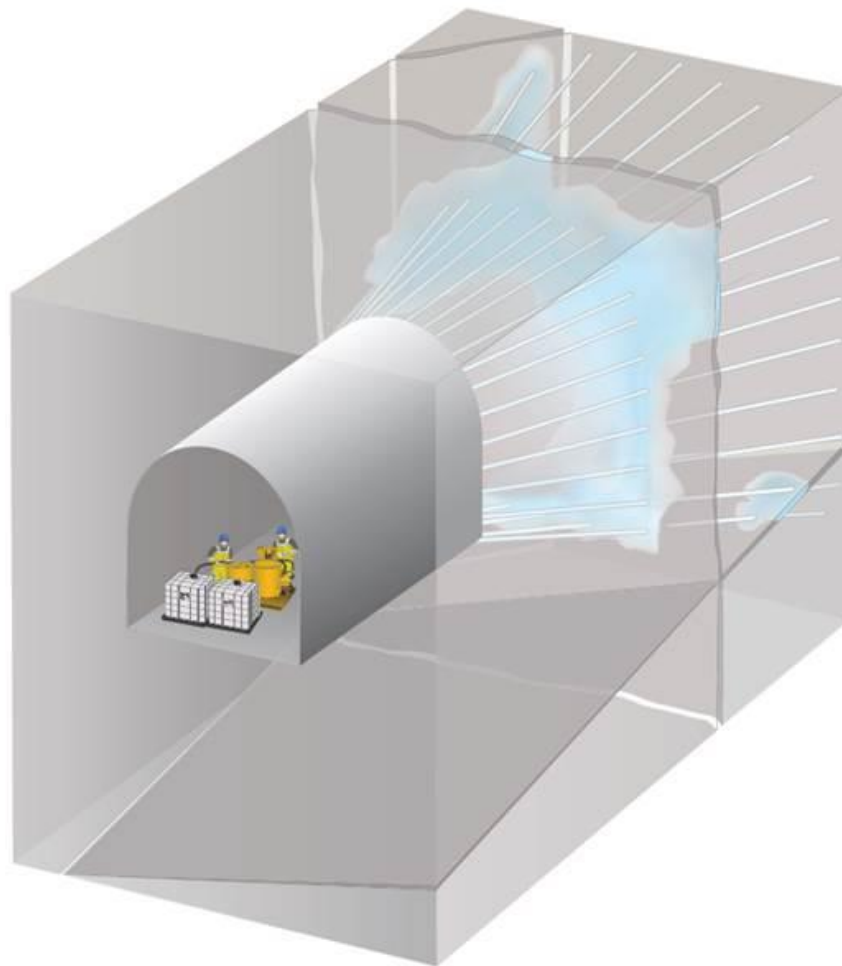
1. Introduction

Nanotechnology has emerged as a key technology in various fields such as electronics, food science, drug delivery and material science (2). Nanomaterials conceived and produced by chemists range wide and far on the periodic table. Nanoparticles are one of the most common types of nanomaterials produced. Often inorganic nanoparticles are based on gold, titanium, iron, or silicon. Due to the prevalence of silicon in the earth's crust and thus low cost of raw material, silica nanoparticles are the most commonly produced nanoparticles. Silica nanoparticles are used in several industrial applications such as food additives, hygiene products, medical products, electronic devices, oil recovery, and recently as grouting material in tunnels and soil stabilization (3-12).

Silica nanoparticles are commonly composed of amorphous silica with the stoichiometric formula SiO_2 . Today a broad range of silica nanoparticle suspensions so called silica sols are produced industrially, with the two biggest manufacturers, in the EU and US, being Nouryon (formerly AkzoNobel) and Grace (formerly Du Pont). Nouryon is known for producing the Levasil while Grace is known for producing the Ludox[®] silica sols. Properties of different commercially available silica sols such as particle size, etc. are given in Table 1 in paper I. Silica sols have a range of properties that make them suitable as a grouting material for sealing leaking fractures in tunnel walls. First and foremost is their ability to form a gel when a salt of sufficient concentration is introduced into the sol. The salt concentration can be varied to achieve gel times from instant gelling up to several weeks. The second property of silica sol is its low viscosity (< 15 cP) which means that it can penetrate fractures with an aperture down to 15 μm (13, 14). Given that silica is common in natural rocks the material is also considered environmentally friendly (15, 16).

These properties of silica sols make them an attractive alternative to the chemical grouts otherwise used for sealing of narrow fractures. Chemical grouts mainly contain a number of polymers e.g. polyurethane, epoxy resins, acrylamide, methacrylate, and acrylate (17, 18). While the polymer material can be considered inert and harmless the monomers needed to form the polymer are highly toxic. The use of chemical grouts therefore risks polluting the ground water and may affect the health of construction workers, where they are used.

For grouting it is common to use a gel time from 30 to 60 minutes, which gives ample time to pump the sol into the rock fractures. Cheap and easily available salts such as NaCl or KCl are used to induce gelling and these are known as accelerators. The silica sol is pumped into boreholes, called a fan see Figure 1, where the sol seeps into the fractures and forms a gel. The tunnel is then extended into the grouted area and if necessary the grouting procedure is repeated into the next tunnel section. This sort of grouting is known as pre-grouting. Post-grouting is also possible where the grouting takes place in an already dug out section of the tunnel. Post-grouting increases the risk of grouting material leaking into the tunnel and is often seen as an emergency measure.



Figur 1: Illustration of pre-grouting where grout is injected into boreholes and spreads into rock fractures. Once grouting is completed the tunnel is extended into the grouted area and the grouting procedure is repeated. Illustration by Karin Holmgren; reprinted with permission from BeFo and first published in BeFo report No. 106 (19).

1.1. Aim

While silica sol has been and is being used as grouting material today, there is little to no experience in how the gel behaves over time. On the other hand, concrete, which due to its low cost is the most common grouting material, is expected to last for 15-115 years (20), depending on material quality and surrounding environment, before maintenance measures are needed; but for silica sols/gels no such number exists. One of the aims of this thesis is therefore to evaluate the longevity of silica gels when these are exposed to waters of different pH and ion compositions typical for groundwater in the presence of cement. Another aim of the thesis is to understand the role of ions at the silica nanoparticle/solution interface in forming gels which is of great interest for the use of silica sols as grouting material. The nature of ions can have significant effect on the aggregation of the silica nanoparticles and thus the formation of gel. Finally this thesis also touches upon the effects of particle size and temperature on the gelling behaviour of silica sols.

2. Background

This part deals with silica sols and the theories used for explaining the behaviour of sols in various environments. It also deals with the behaviour of silica gels but to a rather limited extent.

2.1 Nanomaterials

Nanomaterials have the capability to create a paradigm shift in the technological development within the field of material science. A nanomaterial is defined as a material that has a span of 1-1000 nm in at least one dimension. The nano-size dimensions of nanomaterials lead to the fraction of surface sites being significantly higher than for other types of materials (21). An example of this can be seen in Figure 2 where the surface area for

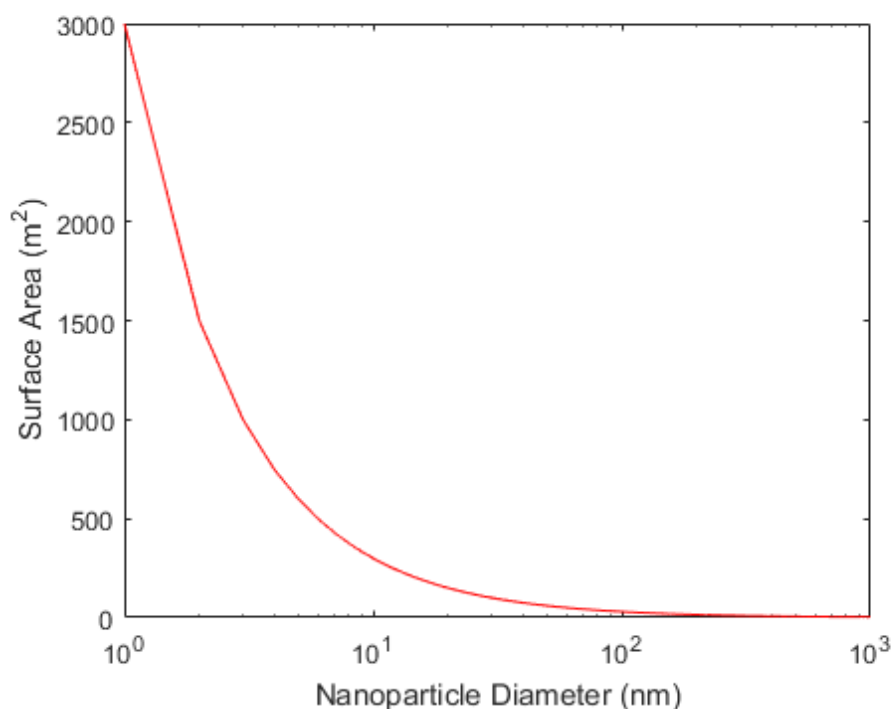


Figure 2: Total surface area for 1 gram of monodisperse nanoparticles with a density of 2 g/cm³ showed versus the diameter of the nanoparticles. The surface area increases rapidly as the diameter of the nanoparticles decrease.

silica nanoparticles is plotted against the diameter of the particles.

Particles of 40 nm diameter have approximately 10% of the atoms located at the surface whereas for 20 nm particles the number of surface atoms is closer to 20% (21). These

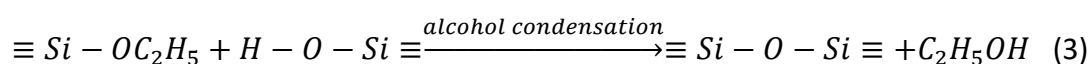
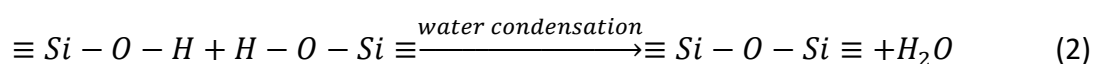
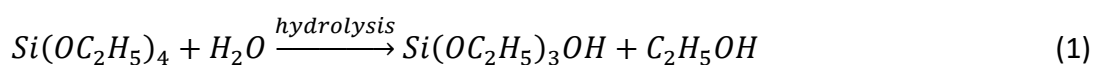
relatively large numbers of surface atoms will affect the properties of nanomaterials. Surface atoms have surface groups which are known to have a higher reactivity than bulk atoms/bonds. Another way to describe it is that the surface atoms have a higher free energy, making them more reactive. For this reason nanomaterials require some sort of stabilization to prevent aggregation. Stabilization can be achieved by a number of methods like surface functionalization, steric stabilization, or electrostatic stabilization (22). What makes nanomaterials special is the flexibility in creating and regulating a large variety of surface phenomenon leading to a large versatility of nanomaterials.

2.2. Silica sols

The word sol is used to describe a solution of solid material often particles in a solvent. It is important to distinguish from a solution where said particles dissolve into single molecules/ions in the solvent. In a sol the particles are not dissolved but suspended in solution.

2.2.1. Production

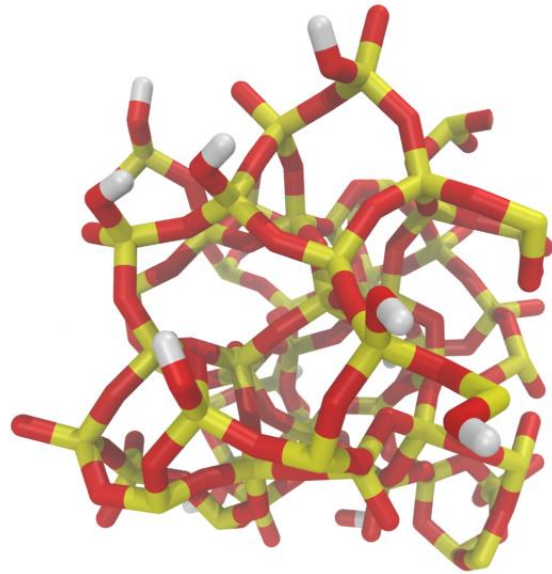
The sol-gel method is the most common method for synthesizing silica nanoparticles and producing silica sols. The method uses polymerization of molecular precursors such as tetraethylorthosilicate ($\text{Si}(\text{OC}_2\text{H}_5)_4$, TEOS) or silicate salts such as sodium silicate (Na_2SiO_3) to form particles (23, 24). The particle formation is achieved through a number of reactions; hydrolysis, water condensation, and alcohol condensation. The reaction steps are given below (equations 1-3) for TEOS precursor (23-27).



Equations 1-3 occur in the presence of a catalyst in the form of an acid or base, typically HCl or NH_3 , and the nature and concentration of this catalyst has been shown to have the highest impact on the kinetics of the reactions (24, 26). Other factors such as the type of molecular precursor, temperature, and pressure may also affect the kinetics. This method forms the basis for the production of silica sols on an industrial scale and is also known as

the Stöber method (25). However, in industrial manufacturing TEOS is often replaced by cheaper silicate salts such as sodium or potassium water glass.

As reactions given by equations 1-3 proceed, the formation of siloxane bonds (Si-O-Si) will lead to the creation of an extensive amorphous silica network. Figure 3 shows a small particle where the silica network is clearly seen. Industrially produced particles typically have an average size of 5-40 nm and are delivered in sols of 15-40 wt% particles. The sols usually have a pH of 9-10 unless some silicon surface atoms have been



substituted by aluminium atoms which lead to the sols being stable at pH values < 8 (28).

Figure 3: Amorphous silica network where yellow = silicon, red = oxygen, and grey = hydrogen.

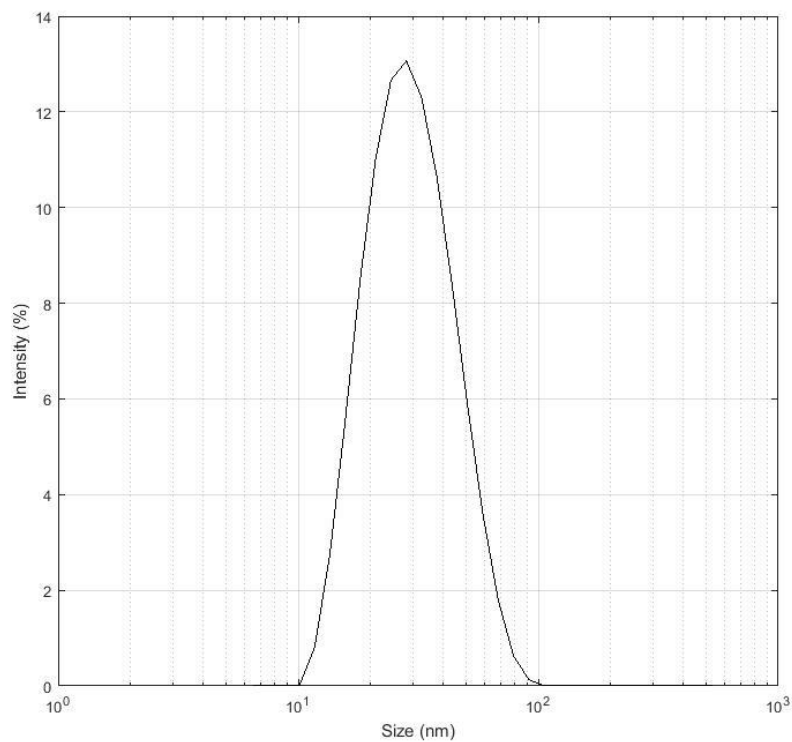


Figure 4: Particle size distribution for Ludox[®]TM-40 silica sol from DLS measurement. The distribution shows a typical lognormal distribution with particle sizes from 10 to 100 nm.

Produced particles are never completely monodispersed in size but the range of the particle sizes can be controlled down to a point. In Figure 4 the size distribution of an industrially produced silica sol as measured by dynamic light scattering (DLS) (see part 3.4. for method details) can be seen. In this sol particles vary in size from 10 nm to 100 nm with the majority of particles having a size of around 30 nm.

2.2.2. Surface Chemistry and Stabilization

The surface groups of amorphous silica are the silanol group ($\equiv \text{Si} - \text{OH}$) or siloxane group ($\equiv \text{Si}_2\text{O}$) (29). Siloxane groups are most prevalent on fumed silica and are not present in any significant number on industrially produced silica sols. They are also chemically inactive in the common pH range (1-14) and thus not involved in any of the surface phenomenon described below (30). The silanol group can protonate and deprotonate depending on the pH of the solution (31-34).



Equation 4 occurs in the pH interval from the point of zero charge (pH 2-4, PZC) up to pH 12 (35). Equation 5 only occurs at pH values below point of zero charge and will therefore not be relevant in this thesis (36).

The silica surface has been shown to contain mainly two types of silanol groups (37, 38). The geminal or vicinal groups are situated only a few Ångström from each other and can therefore form hydrogen bonds between neighbouring groups which helps to stabilize the negative charge formed due to deprotonation, see Figure 5 (39). The isolated silanol groups have a pKa of 8.5-9.9 and constitute 81-85% of the surface groups (38). Geminal or vicinal silanol groups have a pKa of 4.5-5.5 and constitute 15-19% of the surface groups.

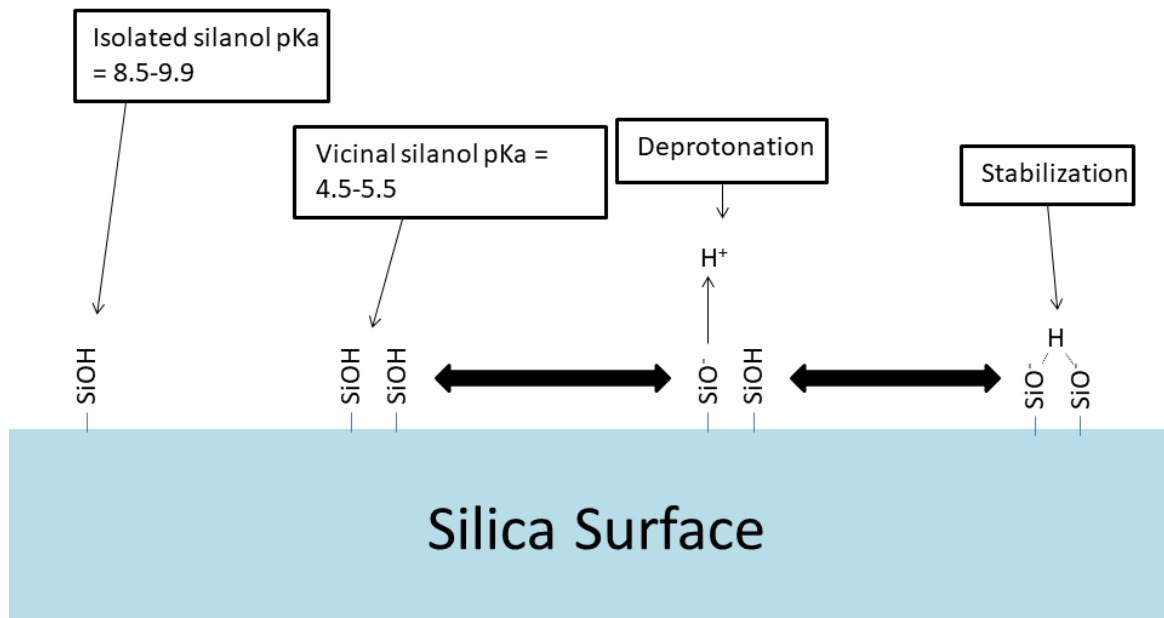


Figure 5: Conceptual picture showing one isolated silanol group and the stabilization course of a vicinal silanol group. The stabilization can also occur for geminal groups ($=Si(OH)_2$).

Deprotonation as described by equation 4 will lead to silica nanoparticles carrying a negative surface charge when the pH is above the PZC. For industrially produced silica sols this negative charge is the main mechanism of stabilization, known as electrostatic stabilization. Two particles approaching each other will be repelled by the repulsive electrostatic forces stemming from the negative surface charge on both particles.

In Figure 6 the zeta potential at varied pH for a silica sol is shown. Zeta potential is a crude measurement of particle stability since it measures the potential at some distance from the surface and not directly at the surface (for a more detailed description of the method see 3.4.). However, the deprotonation of silanol groups leads to higher negative surface charge and a more negative zeta potential which is clearly illustrated by Figure 6.

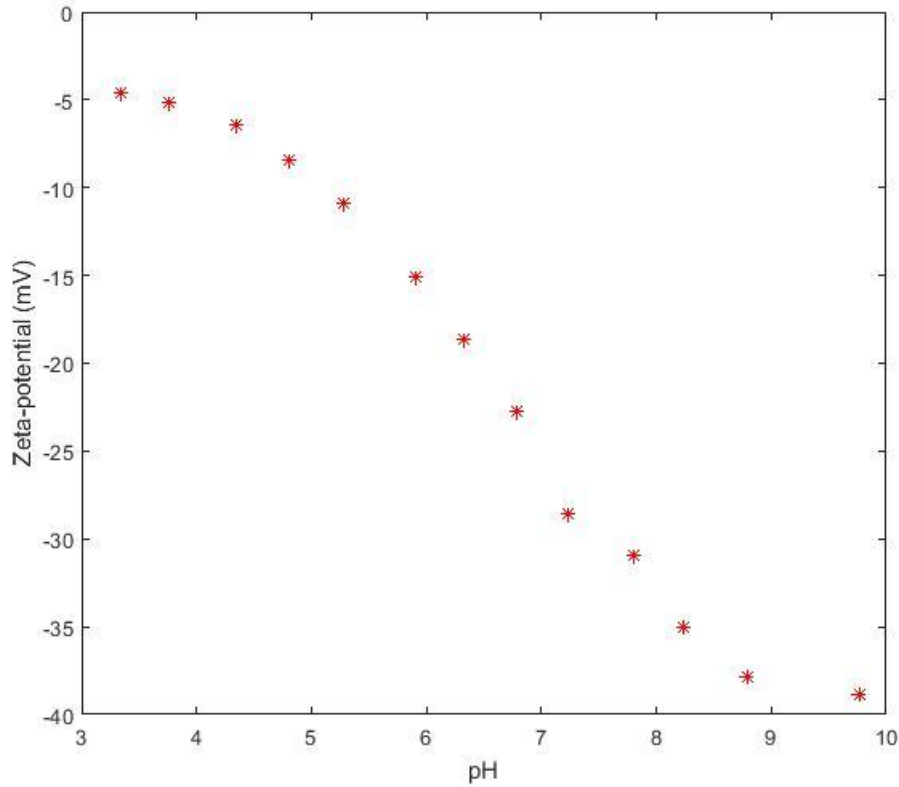


Figure 6: Zeta potential at varied pH for Ludox®TM-40 silica sol. As pH increase the zeta potential clearly decrease.

The electrostatic stabilization of silica sols can be described using the Derjaguin-Landau-Verwey-Overbeek (DLVO) theory. DLVO theory is based on the ratio of repulsive electrostatic potential (ϕ_R) and attractive van der Waals potential (ϕ_A), see equation 7 (22).

$$\phi_{net} = \phi_R + \phi_A \quad (7)$$

The balance of these potentials gives rise to the overall net potential (ϕ_{net}) between two particles. If $\phi_R > \phi_A$ then the ϕ_{net} is repulsive in character and the particles will repel each other. If the opposite occurs where $\phi_R < \phi_A$ the ϕ_{net} will be attractive and the particles will aggregate.

The DLVO theory describes the ϕ_R potential according to equation 8:

$$\Phi_R = \frac{64\pi a n_{\infty} kT}{\kappa^2} \tanh^2 \left(\frac{ze\psi_{\delta}}{4kT} \right) \exp(-\kappa S_0) \quad (8)$$

where a is the radii of the particle, n_{∞} is the number density of the bulk solution (water), k is the Boltzmann's constant, T is the temperature in kelvin, z is the ion valency, e is the

elementary charge, S_0 is the distance of closest approach between the particles, ψ_δ is the surface potential, and κ is the Debye parameter.

The surface potential ψ_δ is difficult to determine and is often estimated as the Zeta potential. The Debye parameter κ can be determined using Equation 9:

$$\kappa = \sqrt{\frac{\sum_i e^2 z_i^2 n_{i,\infty}}{\epsilon \epsilon_0 kT}} \quad (9)$$

where $n_{i,\infty}$ is the number density of ions in the bulk solution, ϵ is the relative permittivity, and ϵ_0 is the relative permittivity of vacuum. κ^{-1} is known as the Debye length and can be seen as the distance at which two particles start to electrostatically repel each other. According to Equation 9 as the valency and/or concentrations of ions in the solution increases the Debye length will decrease and thus the stability of the sol will also decrease, see Table 1. As ion concentration increases the screening of the electrostatic forces will increase which leads to decrease in the repulsive potential (ϕ_s), see Figure 7. Particles can thus at higher ion concentration approach each other without significant repulsion and this is closely connected with the Debye length. The Debye length can therefore be said to be a measure of the repulsive forces between particles dependent on the nature of the ion solution and thereby a measure of the stability of the particles in said ionic solution. A clear limitation of the Debye length is its inability to capture specific ion effects since all ions of the same valency are treated in the same way i.e., ion size is ignored (equation 9).

Table 1: Debye length calculated for 1:1 and 2:1 salts at three cation concentrations. The Debye length shortens when salt concentration is increased due to shielding of electrostatic repulsion potentials.

Concentration Cations (M)	Debye length 1:1 Salt (nm)	Debye length 2:1 Salt (nm)
0.02	2.15	1.76
0.33	0.53	0,43
0.50	0.43	0,35

ϕ_A in the DLVO theory describes contribution from van der Waals forces. These are fluctuations in the electron clouds of atoms which lead to temporary dipoles. One temporary

dipole induces in other atoms dipoles which can lead to weak attractive interactions between atoms and in extension between particles. The van der Waals potential between two particles can be described by equation 10:

$$\Phi_A = \frac{Aa}{12S_0^2} \quad (10)$$

where A is the Hamaker constant. The Hamaker constant is specific for the material of the particles and it incorporates the ratio of the previously mentioned fluctuations in the electron clouds. It can be calculated using equation 11:

$$A = \pi^2 \rho_N^2 B \quad (11)$$

where ρ_N is the molecular density of the material and B is a constant dependent on the polarizability of the atoms and the ground state of the atoms. From this we can conclude that an increase in the Hamaker constant will increase the attractive potential acting between the particles leading to aggregation in sols. This is one of the reasons for the relative high stability of silica sols compared to other oxide sols. Silica has a low Hamaker constant ($6.5 \cdot 10^{-20}$ J) compared with titanium dioxide (TiO_2 : $15.3 \cdot 10^{-20}$) and aluminium oxide ($\alpha\text{-Al}_2\text{O}_3$: $15.2 \cdot 10^{-20}$) (40).

The interplay between ϕ_R and ϕ_A as two particles, with a surface charge, approach each other can be seen in Figure 7. As the particles approach each other both ϕ_R and ϕ_A will increase. However, the rate of force increase is not the same. This gives rise to two attractive minimums called the primary and secondary minimum. The secondary minimum is the point at which the particles are at Debye length distance from each other and the interactions are relatively small. The primary minimum can be seen as the point at which two particles have collided and formed a stable aggregate. In-between the primary and secondary minimums are a maximum in repulsive potential (ϕ_s). Increase in ion concentration leads to decrease in ϕ_s which makes it easier for particles to aggregate.

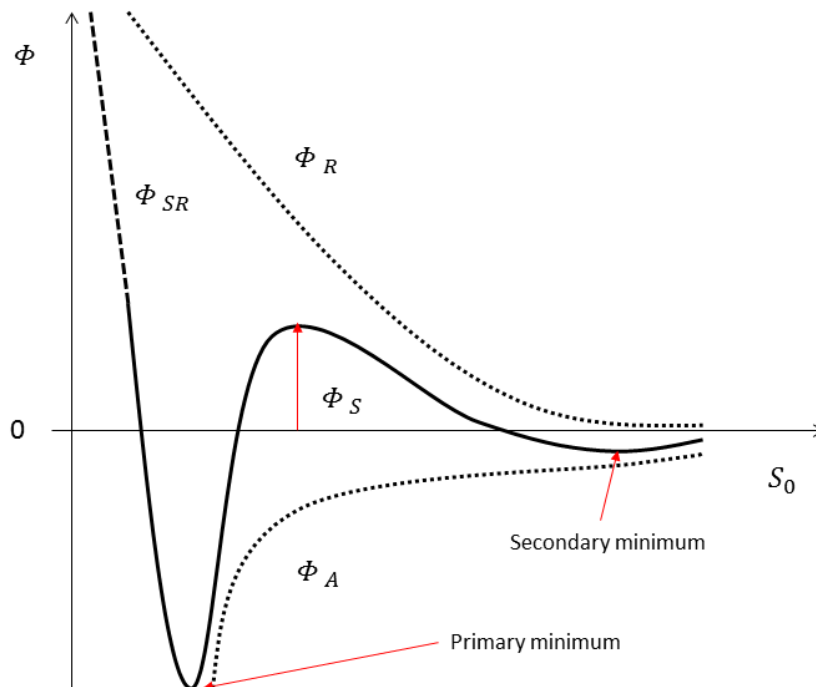


Figure 7: Graph showing the development of electrostatic repulsion potentials (Φ_R) and Van der Waals potentials (Φ_A) by the two dotted lines in relation to the distance between particles (S_0). The solid line represents the sum of Φ_R and Φ_A , with a primary and secondary minimum. Φ_S represent a maximum in repulsive potential which must be overcome by the particle kinetic forces in order for aggregation to occur. Φ_S is reduced by introducing salt to a silica sol.

If the particles continue to move closer to each other past the primary minimum the repulsive forces will increase rapidly. This can be seen in Figure 7 by observing the increase of Φ_{SR} which represents the overlapping of surface atom orbitals.

While the DLVO theory describes the stability of sols rather well it has some limitations in that it only takes into account two main forces (electrostatic and van der Waals). Forces between particles may have other origins and these are not treated by the classical DLVO theory. Examples of such non-DLVO forces, also called X-DLVO, are magnetic attractions, hydrophobic, osmotic repulsion, elastic-steric repulsion, ion specificity, and bridging attraction (41-51). Typical non-DLVO behaviour for silica is the formation of a gel layer of

silicic acid that extends from the silica particles at low pH and results in steric stabilization (52). Silica sols therefore show a stability maximum close to the PZC which is between pH values of 2 to 4.

2.2.3. Interaction of silica surface and ions - Destabilization

As mentioned the silica nanoparticles will carry a negative charge at pH values above the PZC. Most silica sols are kept at a pH of 9-10 and are electrostatically stabilized by the negative surface charge. Cations are attracted by the negative charge on the silica surface and thus interact with the surface. If the ion concentration in a silica sol reaches a concentration above the critical coagulation concentration (ion concentration at which aggregation between particles occurs) the repulsion potential (ϕ_s) as shown in Figure 7 will be reduced to such an extent that it allows aggregation of the particles. This behaviour is further illustrated in Figure 8 by showing the decrease of the Debye length (Debye sphere) as ion concentration is increased as shown in Figure 8 A to B. In silica sol this leads to the formation of a silica hydrogel, within a certain time known as the gel time. The gel time can be controlled by changing the concentration of ions in the silica sol.

The ions that approach closest to the silica surface form a layer known as the Stern layer (53, 54). The outer border of this layer is known as the slipping plane, see Figure 8. The ions in the Stern layer are limited in their diffusivity due to the strong interactions with the silica surface. The major contribution in screening the negative surface charge is from ions in the Stern layer.

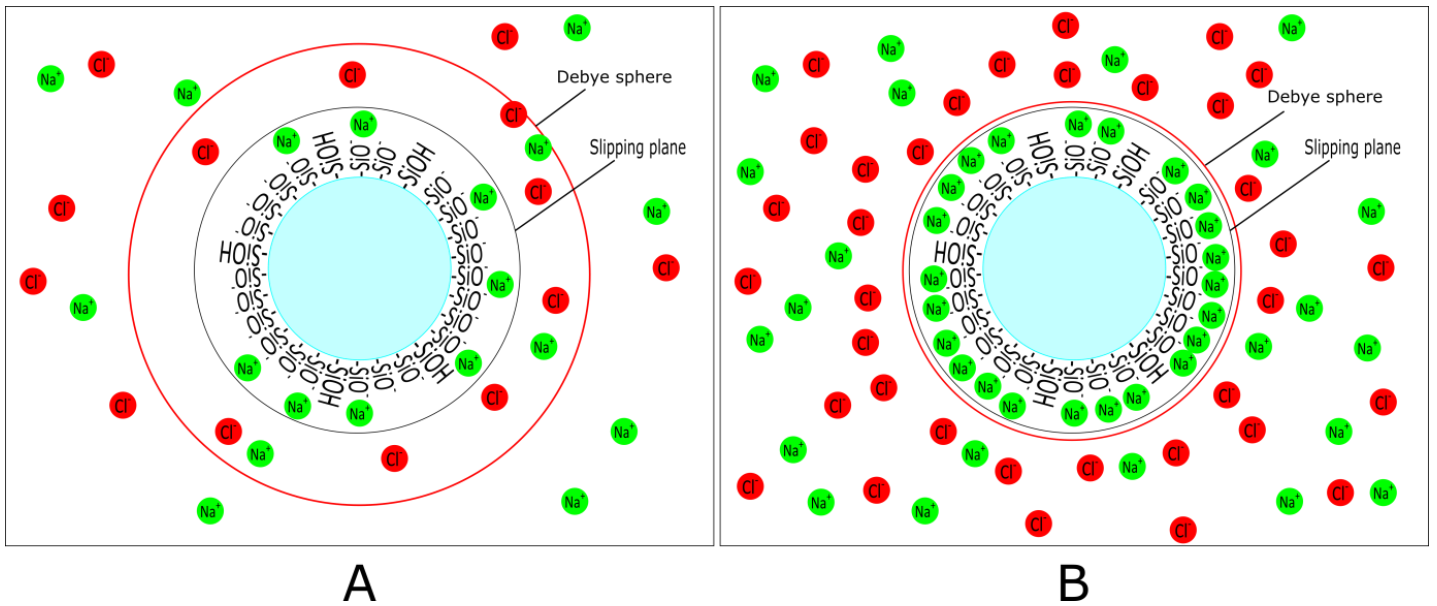


Figure 8: Traditional illustration of the ion interaction with silica surface and its effect on the Debye length where (A) silica particle in a low ion concentration leading to relatively few cations adsorbing to the silica surface compared to (B) where the ion concentration has been increased leading to a reduction in Debye length indicated by the Debye sphere. The slipping plane indicated the interface between the stern layer and the diffuse layer and remains the same in both cases.

The large amount of cations in the Stern layer as shown in Figure 8B will lead to anions being attracted. This leads to the formation of a diffuse layer of ions stretching out from the silica surface. The Gouy-Chapman theory provides the relationship between the surface charge and the distribution of ions in the diffuse layer and is based on Poisson-Boltzman statistics (55, 56). In the diffuse layer the ion concentration is higher than in the bulk and ions are free to diffuse in and out of the layer.

Cations can thereby lead to the destabilization of the silica sol and result in the aggregation of nanoparticles and formation of a gel. However, different cations do not adsorb equivalently in the Stern layer. The adsorption follows the concept of Hofmeister series. The Hofmeister series is coined after the historic paper “Zur lehre von der wirkung der salze” by Franz Hofmeister in 1888, where he compared the ability of salts to precipitate egg-white proteins from a solution (57). He noticed that some salts are more effective in propelling precipitation. It gave rise to the terms of salting in and salting out regarding proteins stability

in solutions. Since its conception; Hofmeister series has been discovered not only for proteins but also for a wide range of surfaces.

For amorphous silica surfaces the cations of the alkali metal salts have been shown to follow the direct Hofmeister series (58, 59). The adsorption of monovalent alkali ions thus follow: $\text{Li}^+ < \text{Na}^+ < \text{K}^+ < \text{Rb}^+ < \text{Cs}^+$. This is valid for pH ranges up to 11; above pH 11 the series has been shown to reverse so that Li^+ adsorbs strongest and Cs^+ weakest (60). The explanations for the specific ion adsorption at the silica/solution interface are twofold. The first is related to the polarizability of the cations. Li^+ is a small ion with a crystallographic, so called bare, radius of 1.02 Å (61). This small size of the electron cloud leads to strong interactions between the core protons and the two electrons which lead to the Li^+ ions being less prone to polarization. In contrast Cs has a bare radius of 1.70 Å (61). Cs^+ has a larger electron cloud and thus can be more easily polarized than Li^+ . The polarizability of ions will affect their ability to interact with the negatively charged silanol groups on the silica surface. The field generated by negatively charged surface will easily induce polarization in the larger Cs^+ ion which can thus interact more strongly with the silica surface.

The second explanation is the formation of a structured water layer around some of the ions. Just as the previous explanation for the Hofmeister series this is based on the size of the ions. The small Li^+ ion leads to a relatively large charge density of $0.22 \text{ e}/\text{Å}^3$ (61). The charge density will attract polar water molecules, leading to Li^+ having 8-10 structured water molecules surrounding the ion (62, 63). The surrounding water layer swells the radius of the ion so that it has a hydrated radius of 3.58 Å (64). In comparison the much larger Cs^+ ion has a charge density of $0.05 \text{ e}/\text{Å}^3$. The low charge density leads to Cs^+ not attracting as many water molecules and the hydrated ion has a hydrated radius of 3.29 Å, which is smaller than Li^+ . The water layers surrounding the ions have led to the concept of structure maker and structure breaker ions. Li^+ and Na^+ are considered structure maker ions because they are small enough to form a structured layer of water around them. The number of strongly bound water molecules as determined by dielectric relaxation spectroscopy are for Li^+ and Na^+ 8-12 and 4.5, respectively (63). K^+ , Rb^+ , and Cs^+ are large enough that they do not form a structured water layer. The observed ion-solvent interaction number is 0 for both K^+ and Cs^+ indicating no strongly bound water layer (63). This means that structure maker ions are unable to interact closely with the silica surface since the water layer is in the way. However,

structure breaker ions do not have a water layer and can thus adsorb closer to the silica surface. This offers some explanation to the Hofmeister series but it is probable that both effects discussed here (polarizability and hydration layer) play a part in the ion specific adsorption at the silica solution interface.

Divalent cations adsorb stronger than the monovalent cations due to the higher charge density. The most tested ions for the silica surface in this group are Mg^{2+} and Ca^{2+} since these ions are common both in the earth crust and also in groundwater. It has been shown that these two ions follow the series $Mg > Ca$ when interacting with a silica surface (58). This is the opposite than the direct Hofmeister series for the monovalent ions. The shift is strange because it goes against the two previous explanations given above for the direct Hofmeister series. Ion-solvent interaction measured by dielectric relaxation spectroscopy indicate that Mg^{2+} and other poly-valent ions have a second and sometimes even a third hydration shell (63). Mg^{2+} is smaller and has more ordered water molecules surrounding it than Ca^{2+} and should thereby follow the direct Hofmeister series. To the knowledge of the author no explanation is given in the current literature for this shift.

2.3 Aggregation of silica sols – Gelling mechanics

Gelling can be induced in silica sols by two main methods; changing the pH or introducing ions into the solution. Silica sols have two stability maximums, one at pH 2-4 and the other at pH > 8. In-between these maximums i.e., in the pH range 4-8 the electrostatic forces are not strong enough and the pH is not low enough for the formation of a silicic acid gel layer, which results in the aggregation of silica (29). However, the aggregation using pH change is generally slow whereas faster aggregation can be achieved using ionic solutions. For monovalent ions the efficiency in inducing gelling follows the Hofmeister series; $Li^+ < Na^+ < K^+ < Rb^+ < Cs^+$ (1). For divalent ions Mg^{2+} is the most effective in inducing gelling followed by Ca^{2+} at pH values > 9. Furthermore, the salt concentration can be varied in order to achieve a predetermined gel time.

Industrially produced silica sols, usually have particles smaller than 100 nm. The main movement of particles in such sols is due to Brownian motion, which is random motion due to fluctuations in solvent molecules impacting the particle surface. The movement of particles will lead to particle collisions and these may result in formation of aggregates if the

attractive forces are strong enough. There are two regimes by which silica particle aggregation can proceed. These are known as reaction limited cluster aggregation (RLCA) and diffusion limited cluster aggregation (DLCA) (65-67). In RLCA not all collisions lead to the formation of an aggregate. In this regime the ion concentration in the silica sol is not enough to completely overcome the electrostatic barrier as shown in Figure 7. Since not all collisions lead to aggregate formation the gel time of RLCA is longer than for DLCA. The aggregates formed by RLCA tend to be more compact than those formed by DLCA. This since the formation of aggregates requires the minimization of surface area of the nanoparticles and thereby a reduction in surface energy, see Figure 9. Aggregates formed will therefore be shaped in order to reduce surface area of the nanoparticles, that is, minimize the number of surface groups present in the aggregate. In the DLCA regime every collision leads to the formation of aggregates since the ion concentration is large enough for the electrostatic forces to be completely screened. For silica sols this regime results in the instant formation of a gel.

The formations of a gel structure from particles is generally considered to follow the fractal gel model (68, 69). Fractal/aggregate dimension can be described using equation 12 where N_d is the number of particles of radius a in the fractal of radius R , and d_f is a fractal scaling parameter (69-71).

$$N_d \approx \left(\frac{R}{a}\right)^{d_f} \quad (12)$$

As aggregation commences the particles will form ever increasing number and size of fractals which will eventually combine to form a continuous gel network.

2.4 Silica gels

Research related with properties of the silica gels is relatively less compared to the research conducted on nanoparticle properties. It has been shown that the properties of the gels depend on the size of the particles, the concentration of the particles in the sol, the pH, the temperature, and mechanical forces e.g. shear forces during gelling (18). As particles gel they form a continuous network of aggregates. The point of the network formation is the gel point, but particles continue to be added to the network even after the gel point. This means that the strength of the gel continue to increase after the gel formation. The formation of a

gel network leads to the formation of pores through which water must navigate in order to pass through the gel. The more extensive the gel network is the harder it will be for water to pass through the gel. Silica is known to increase in solubility as pH increases above 10 (72). It can therefore be assumed that silica gels will dissolve faster as pH increase.

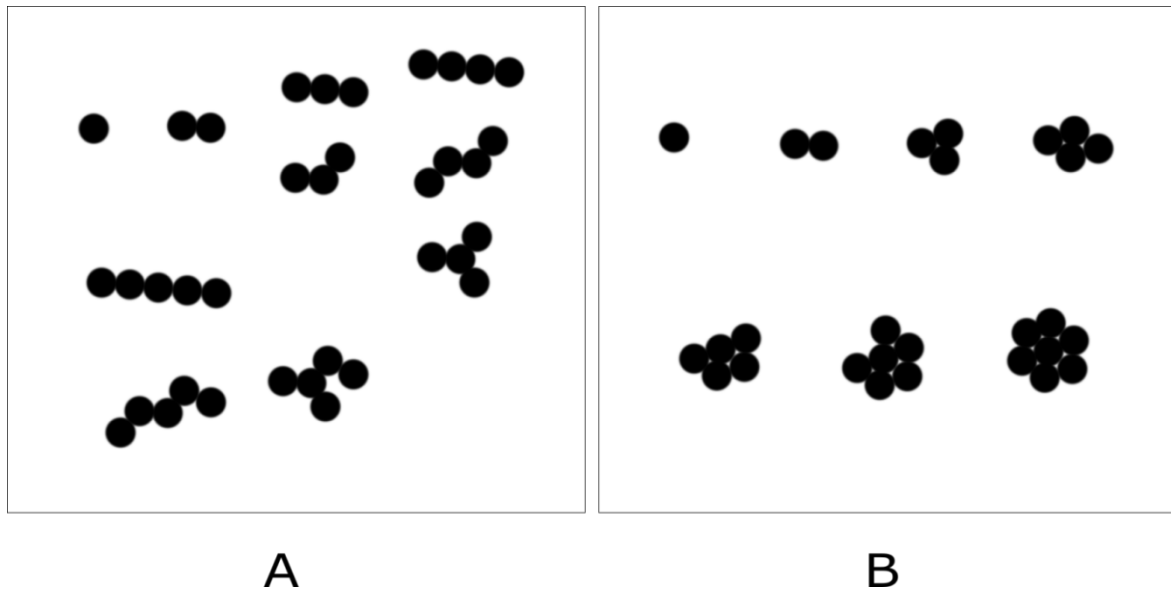


Figure 9: A) shows aggregate types mainly present in DLCA and B) shows aggregate types mainly present in RLCA. Clearly aggregates from B will form a denser gel than aggregates from A.

3. Methods

Here methods and equipment used to produce the results in paper I-VI are presented.

3.1. Gel time tests

For the determination of gel time for destabilized silica sol there exist two methods. A rheometer can be used to decide the so called Winters-Chambon criterion. The rheometer measures the loss modulus (G'') and the storage modulus (G') through oscillating tests. The point at which these two cross where $G''(\omega) \approx G'(\omega) \approx \omega^n$, for a frequency ω , is taken as the gel point. The material is placed in-between two plates and one or two of the plates is rotated back and forth. More on rheometer measurements can be found in part 3.6.

For a gelling material the loss modulus is present to start with, i.e. the material behaves as a liquid. As the gelling proceeds and the continuous network start to form the storage modulus will start to increase. When the storage modulus passes the loss modulus the material can be said to mostly have the properties of a solid material and can thus be

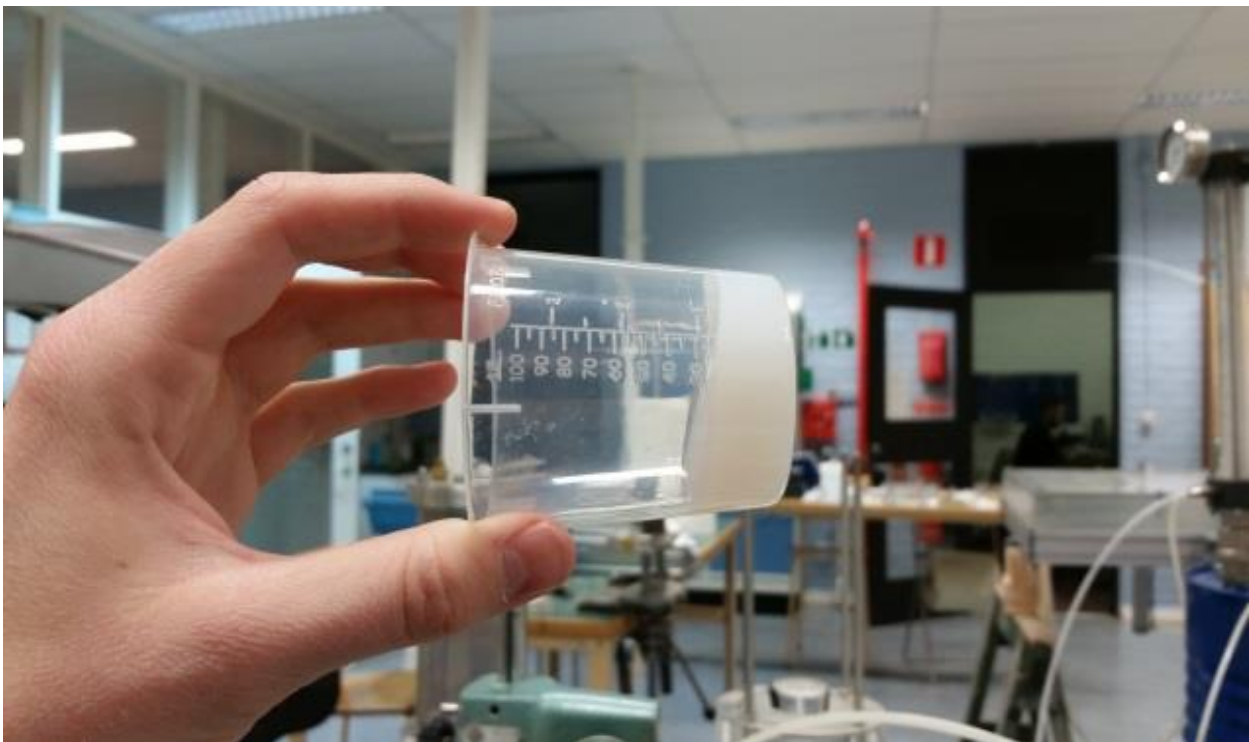


Figure 10: Silica sol in the process of gelling. This sol/gel is close or at the gel point since it is not flowing when the container is tipped 90°.

considered to have formed a gel.

Another and simpler way of measuring the gel time is the so called visual method (this method is the main way of determining the gel times used in this thesis and the papers presented here-in). Here a sol is allowed to gel in a transparent cup or Falcon-tube. The gel time is taken when the sol no longer flows when the container is tipped 90°, see Figure 10. This method is quick and easy but might differ a bit dependent on who performs the test. The difference between the Winters-Chambon method and the visual method has been shown not to be significant (73). When used in this thesis, 15 mL of silica sol is placed in a Falcon-tube. A certain volume of salt solution (often 2M) is introduced into the sol and a timer is started. The tube is kept under close observation until the sol has gelled.

3.2. Potentiometric titration

A method of measuring the interactions between the silica surface and ions is potentiometric titration. Since adsorption of cations to the silica surface facilitates

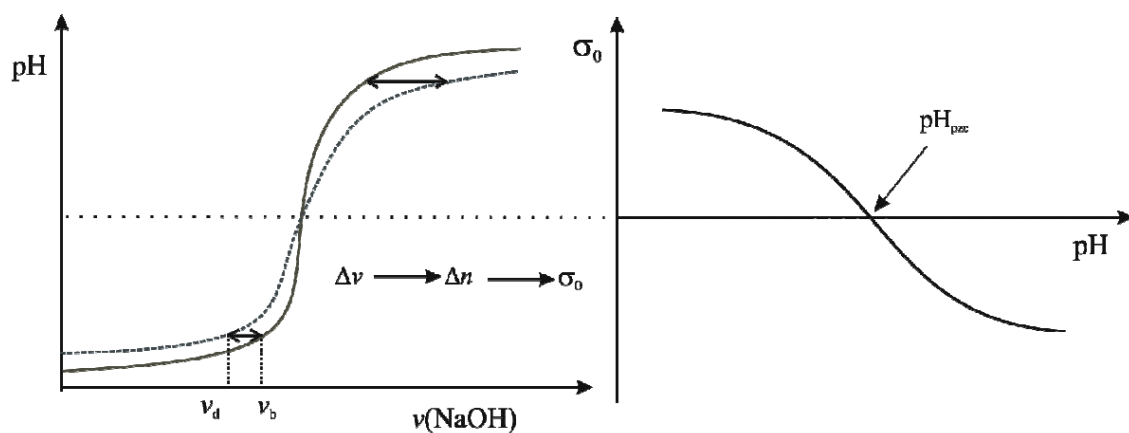


Figure 11: (Left) The solid line shows a typical titration curve for background sample where no colloids are present as NaOH is introduced and pH increased. The dotted line show titration curve for colloidal sample. When colloids are present the curve is shifted as protons dissociate from the silica surface. This shift represents a difference in volume v_b and v_d which can be used to calculate the surface charge density. (Right) Shows typical surface charge density curve for colloidal sol shown as a function of pH. Figure reprinted in accordance with Creative Commons Attribution 4.0 International License (CC BY 4.0 : <https://creativecommons.org/licenses/by/4.0/>) from paper by J. Lützenkirchen et al (1).

deprotonation of the silanol groups (equation 4) it is possible to compare titration on silica nanoparticles with a reference (pure milli-Q water). The difference in added acid or base volume between the sample and reference corresponds to the number of protons released

or adsorbed to the silica surface, see Figure 11. Using equation 13 the surface charge density of the nanoparticles can be calculated:

$$\sigma = \frac{F * C_{HCl}(v_b - v_d)}{s * \gamma * V} \quad (13)$$

where F is the Faraday constant, C_{HCl} is the acid concentration, v_b is volume of acid in the background solution, v_d is the volume of acid in the sample solution, s is the specific surface area of the nanoparticles, γ is the mass concentration of nanoparticles, V is the total volume of the sample (1). Using this method the PZC of the particles must be set manually and for results presented in this thesis the PZC has been set to pH 4.

When measuring the effect of ions on the surface charge density of nanoparticles in the presence of different salts it is important to do the titrations with an acid that corresponds with the salt. Since the effect of monovalent cations has already been extensively researched, this thesis will focus on the effect of anions (58). For chlorides, nitrates, and sulphate salts the corresponding acids used are HCl, HNO_3 , and H_2SO_4 .

A number of salts were titrated in the presence of 2 wt% Ludox TM-40 silica sol. These salts were NaCl, $NaNO_3$, Na_2SO_4 , KCl, KNO_3 , and K_2SO_4 . 75 mL of sample was first purged with N_2 gas for 10 minutes and then titrated with 0.1M NaOH/KOH to a pH of 10. After this the sample was titrated down to a pH of 3 using 0.1M of the corresponding acid. An auto titration device (Titrand 905) with a Unitrode easyClean (Metrohm) glass electrode was used for the titrations. The titrations were conducted in an inert N_2 atmosphere and the temperature was kept constant at 25°C.

3.3. Molecular dynamics simulations

As computers have become more and more powerful in accordance with Moore's law the simulation of atomic and molecular behaviours using a range of computer programs and methods has become more popular (74). One of the simulation methods used is molecular dynamics (MD) simulations where the behaviour of a system of up to thousands of molecules is surveyed using predetermined force fields and vector calculations. It has been shown to be an effective method to follow the behaviour of organic molecules at the silica interface as well as the behaviour of ions around silica nanoparticles (75, 76).

In this thesis results from MD simulations are shown which has used the Gromacs (version 2018.2) in an NVT ensemble to run the simulations (77). CHARMM force field (78) and TIP4P water (79) was used for the simulations. The generated amorphous silica surface had a surface group density of 4.7 OH groups per nm². These groups were either 9% or 18% deprotonated corresponding to pH 6-7 and 9, respectively. A small number of water molecules were randomly replaced by the cations and anions of the salt of interest. A production run was 100 ns giving ample time for the salt to equilibrate at the silica surface. The main purpose of these simulations was to investigate the behaviour of ions at the silica surface, especially for mixed ion systems containing two different types of cations.

3.4. Dynamic light scattering

Dynamic light scattering (DLS) is a method used to measure the size of nanoparticles. The method uses the Brownian motion of particles in tandem with the Stokes-Einstein equation to measure particle size (80). A DLS instrument uses a laser to measure the scattering of light by the nanoparticle. Usually the scattered light is picked up by a detector in the form of backscattered light at 175°. The instrument will send out a number of light pulses and follow the change in intensity between the different pulses. This changed intensity over time is used to create a correlation function. Small particles are known to diffuse faster which is described by the larger diffusion constant derived from the Stokes-Einstein equation, see equation 14;

$$D = \frac{k_b T}{6\pi\eta r} \quad (14)$$

where D is the diffusion coefficient (m²/s), k_b is the Boltzmann's constant, T is temperature (Kelvin), η is the dynamic viscosity (Pa*s), and r is the radius of a spherical particle.

The faster particles diffuse, the faster the correlation function will decay and from this the size of the particles can be calculated. While the DLS method is a fast and an easy way to determine the size of nanoparticles it has a tendency of overestimating the presence of large particles. This is due to the fact that the scattered light intensity follows $I \approx d^6$ where I is intensity and d is diameter of the nanoparticle scattering the light. This means that large particles scatter a million times more light than particles ten times smaller. Scattered light from large particles can therefore easily mask the light from smaller particles which will lead to a shift in the size distribution, given by the instrument, towards the larger particles.

A DLS instrument can also be used to determine the so called Zeta-potential (ZP) of nanoparticles. By using special cuvettes equipped with gold electrodes it is possible to apply a potential to the particle solution. Since nanoparticles carry a surface charge they will start to move according to the applied potential. The DLS instrument can follow this electrophoretic movement and ZP is calculated from the measured dynamic mobility of the particles, which is correlated to the surface charge of the particles. The exact position of the plane at which the ZP is measured is not defined but it is said to be the potential at or slightly outside the slipping plane, see Figure 12.

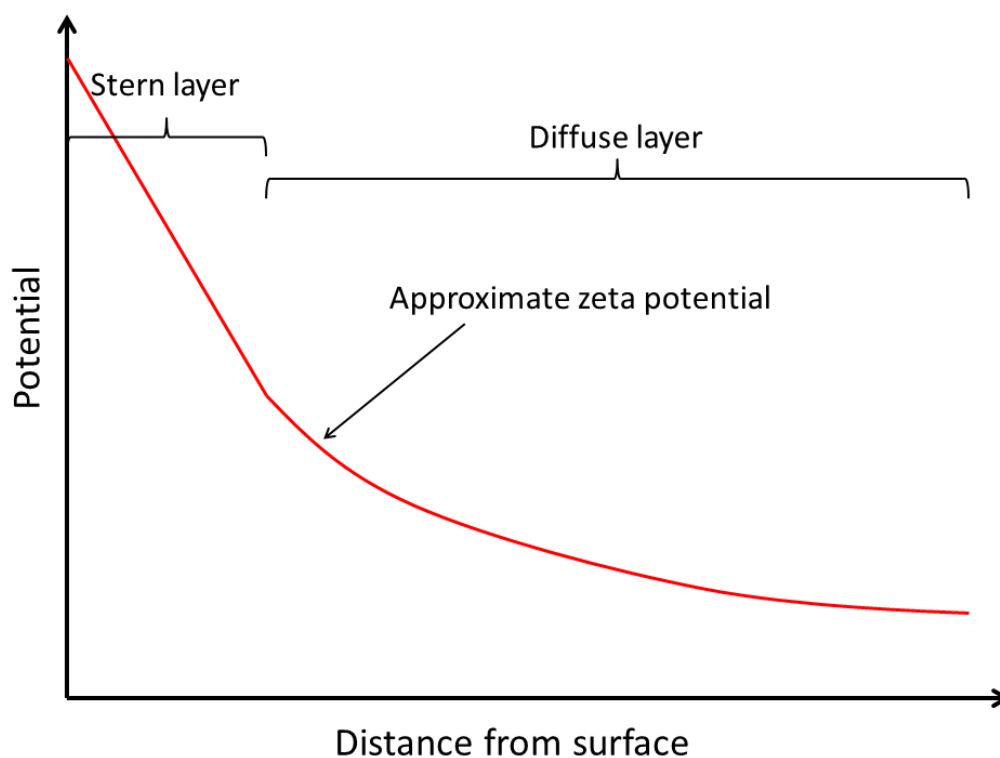


Figure 12: Show potential change from the surface. The stern layer, diffuse layer, approximate position of the zeta potential is included.

Below is given the Henrys equation (equation 15) which can be used to calculate the ZP:

$$u_E = \frac{2\epsilon\epsilon_0\zeta}{3\mu} C(\kappa a) \quad (15)$$

where u_E is the electrophoretic mobility, ζ is the zeta potential, and μ is the viscosity (22).

Equation 15 contains a coefficient $C(\kappa a)$ which is dependent on the Debye parameter (κ) and

particle radius (a). At low salt concentrations this coefficient becomes 1.0 and the equation is referred to as the Hückel equation. At intermediate salt concentrations $0.1 < \kappa a < 200$ the coefficient varies between 1 and 1.5 and the Henrys equation is valid. At high salt concentrations $C(\kappa a) = 1.5$ and the equation is referred to as the Smoluchowski approximation. For all measurements presented in this thesis and the appended papers the Smoluchowski approximation has been used to calculate the ZP.

3.5. Electrospray scanning mobility particle sizer

An alternative to the DLS method is the electrospray scanning mobility particle sizer (ES-SMPS) method. The method uses an electrospray to generate an aerosol which is then lead into dynamic mobility analyser (DMA) which creates a monodisperse stream of particles and these are counted by condensation particle counter (CPC), see Figure 13. The range of particle size detection in the monodispersed stream is varied by changing the electromagnetic field in the DMA. The DMA thus scans through the different sizes of the particles and the CPC counts the number of particles of each size. In the CPC the particles pass through a chamber with saturated butanol. The butanol condenses on the particles surfaces and the particles grow in size. The growth in size makes it possible for a laser to count the number of particles passing through the CPC. When the measured number of particles for each monodispersed flow of particles is combined we get the overall particle size distribution of the particle sol.

In general, samples were diluted to 0.0025 wt% in 20 mM ammonium acetate buffer before ES-SMPS measurements. The pH of the buffer was adjusted using ammonia or citric acid. The electrospray unit was either a TSI model 3480 electrospray aerosol generator or a TSI 3482 electrospray aerosol generator. The capillary in the electrospray was either a silica capillary with OD 150 μm and ID 25 μm or a PEEK capillary with OD 1/16" and ID 25 μm . The SMPS unit was a TSI series 3080 electrostatic classifier or a TSI 3082 electrostatic classifier, both equipped with a DMA model 3085.

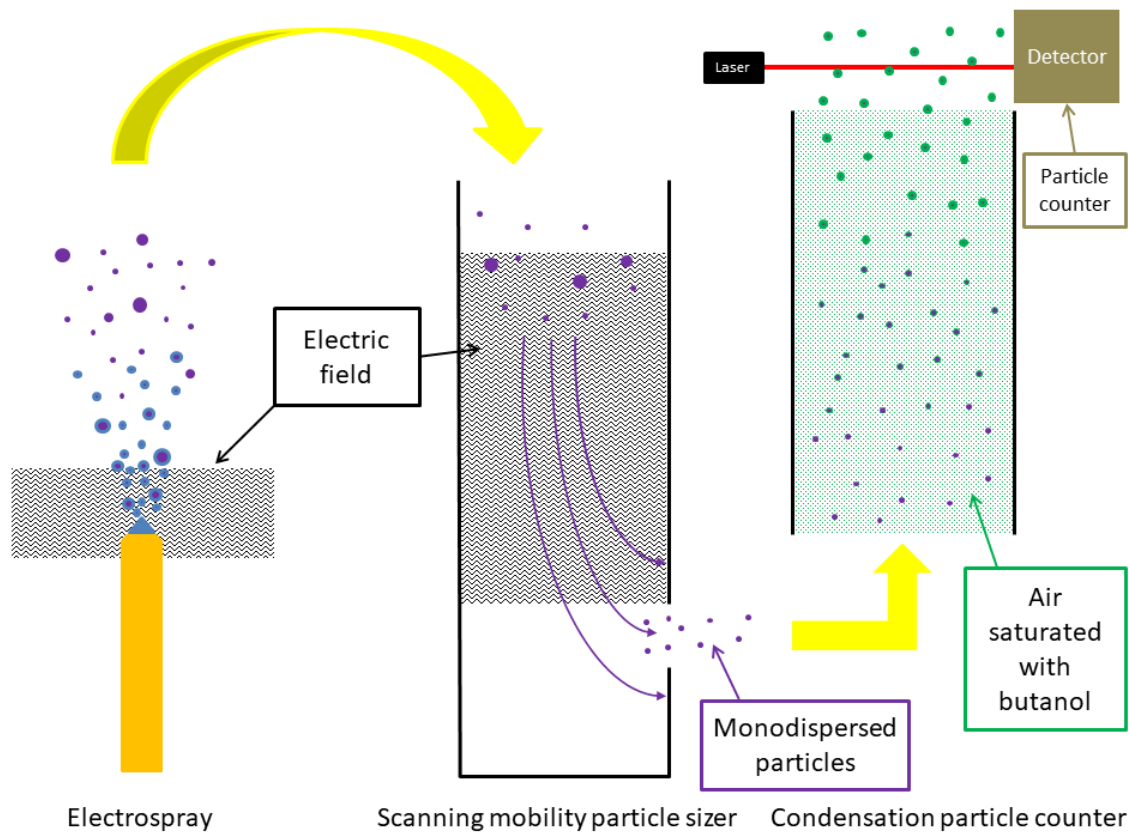


Figure 13: Overview of the crucial parts of the ES-SMPS method.

3.6 Rheological measurements

The rheological tests were introduced in part 3.1. where the measurement of gel time is discussed. Here the details of rheological measurements are presented for the results presented in article V. A MCR-500 (Anton-Paar) rheometer instrument was used to follow the gelling of silica sols at different temperatures. Oscillatory measurements using a CP25-1 cone with a 1° angle and a plate gap of 0.05 mm were conducted. The measurements settings were such that an amplitude tau of 5 Pa with a frequency of 1 Hz was used. An induction temperature plate was used to keep the temperature constant during measurements. Gelling of silica sol was started in a similar manner to gel time tests but the sample was immediately put between the measurement plates in the rheometer and the instrument started measurement within 2 min from the point where gelling was induced.

The main purpose of oscillatory measurements in general is to follow samples viscoelastic behaviour. The sample is sandwiched between two plates where the upper plate is moving and the lower plate is stationary. The instrument measures the complex modulus G^*

($G^* = G' + iG''$, where $i = \sqrt{-1}$) (81). The storage modulus (G') is defined as the part of the shear stress that is in phase with the strain. The storage modulus relates to kinetic force being induced on the material but instead of permanently deforming the material the energy is stored in the material. A material with only storage modulus will resume its previous shape once the exposure to the kinetic force ceases. The loss modulus (G'') is defined as the imaginary part of the complex modulus. The loss modulus can be seen as the force needed to permanently deform a material. The energy used for this is thus not stored in the material but instead used for the deformation. A material with only loss modulus will only deform and not show any elastic properties. The upper plate of the instrument moves back and forth and this movement is described as sinusoidal moving from 0° to 90° at maximum strain back to the plates starting position at 180° to maximum strain in the opposite direction at 270° and coming full circle back to the original position at 360° (82). The maximum height of the resultant sinus curve is taken as the maximum strain (90° and 270°) or deformation amplitude γ_A . The time it takes for the sinus curve to move full circle correspond to the frequency of the oscillation. The force required for the lower stationary plate to stay stationary at maximum strain is measured and taken as the shear stress amplitude τ_A . From the deformation amplitude and shear stress amplitude the so called complex shear modulus is calculated from equation 16:

$$G^* = \frac{\tau_A}{\gamma_A} \quad (16)$$

For a completely rigid sample, such as a solid metal or mineral (ideal elastic materials), the sinusoidal response to the top plates sinusoidal movement would be immediate i.e. the energy transfer to the bottom plate is immediate and there would not be any shift or delay in the response of the material. However, most materials or solutions show some degree of viscoelastic behaviour where the response is not immediate. The result of the top plates sinusoidal movement on the material is a delay in the materials response and the thus we get a phase shift i.e. there is a time lag between the materials sinus curve and the applied sinus curve. Given that the sinus-curve movements are defined in degrees we can also define this time lag in degrees between 0 and 90° phase shift δ . An ideal elastic material will show no phase shift with $\delta = 0^\circ$, an ideal viscous material will show a phase shift of $\delta = 90^\circ$, and a viscoelastic material will show $0^\circ < \delta < 90^\circ$.

Now going back to our previously established complex shear modulus this can be divided into a storage modulus G' and a loss modulus G'' . Imagine the storage modulus as a vector extending from origo with an angle of δ from the x-axis, see Figure 14. Remember from part 3.1. that $G^*=G'+iG''$, where $i=\sqrt{-1}$. The extension of the vector on the x-axis in Figure 14 is thus defined as the storage modulus G' in Pa, while the extension on the y-axis is defined as the storage modulus G'' in Pa. In general the storage modulus can be said to correspond to the part of the sample acting as a solid and the loss modulus to the part acting as a liquid.

From rheological measurements it is also possible to measure the complex viscosity, where $\sigma(t)$ is the shear stress at time t and $\dot{\gamma}(t)$ is shear rate at time t (81).

$$\eta^* = \frac{\sigma(t)}{\dot{\gamma}(t)} \quad (17)$$

We have mainly focused on observing the complex viscosity development for gelling sols when conducting rheological measurements. A standard program from Anton Paar specifically designed to follow gelling procedures was used where the instrument automatically varies the deflection angle during the oscillations to minimize impact on the sample and breakup of the forming gel structure.

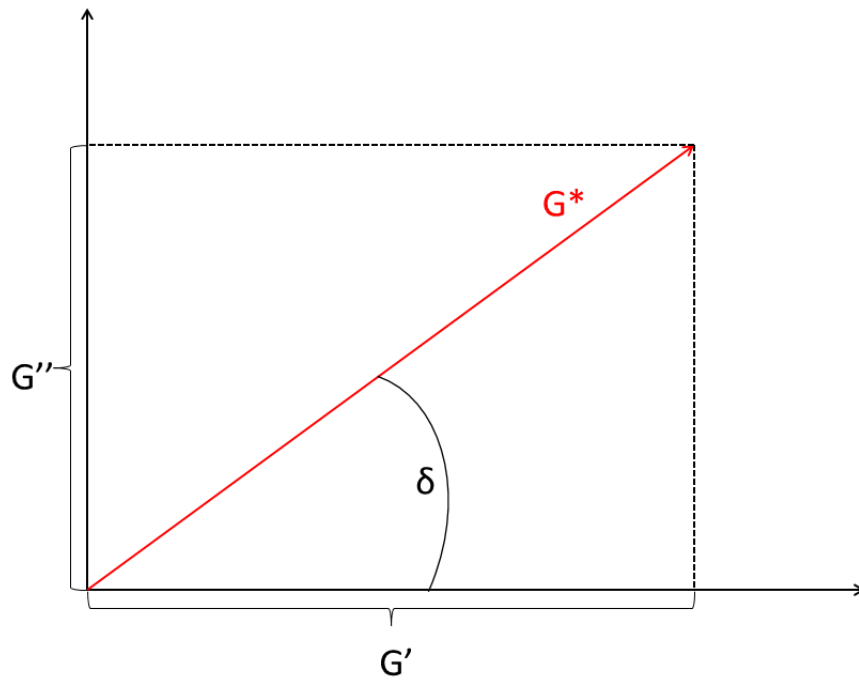


Figure 14: Vector diagram showing the extraction of storage modulus G' and loss modulus G'' from the complex shear modulus vector G^* .

3.7. Long term gel stability tests

In this part the design and setup of long term stability tests for silica gels is described. The methods used here are mainly presented in paper VI. As analysis method inductively coupled plasma was used; this is described in part 3.8.

3.7.1. Design of test equipment

To test the stability of silica gels new test equipment was designed and built. The equipment was designed so that water would pass through a 100 mL block of gel. To prevent water from only flowing along the cylinder walls in the interface between the gels and the cylinder, 3D printed plastic filters were put at the bottom of the cylinder, see Figure 15. These filters only

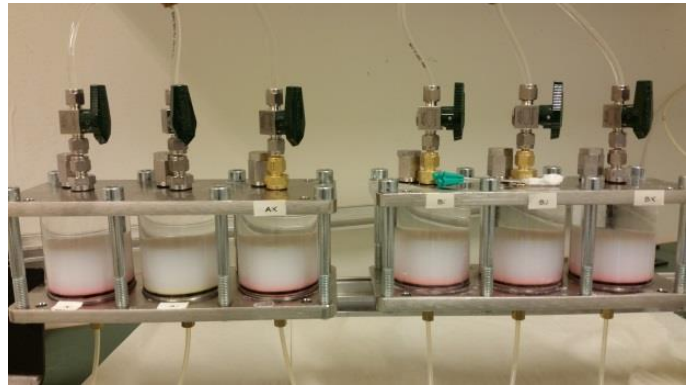


Figure 15: Sample cells sitting in pairs of three. The gels can be clearly seen and the 3D printed plastic filters.

allow water to flow about 1 cm into the centre of the cylinder and thus increase the water gel interactions by preventing water from only flowing along the cylinder sides. The sample cells sit in rows of three which each receive the same kind of water. When the water has passed through the cylindrical sample cells it is collected in plastic vials, see Figure 16. In

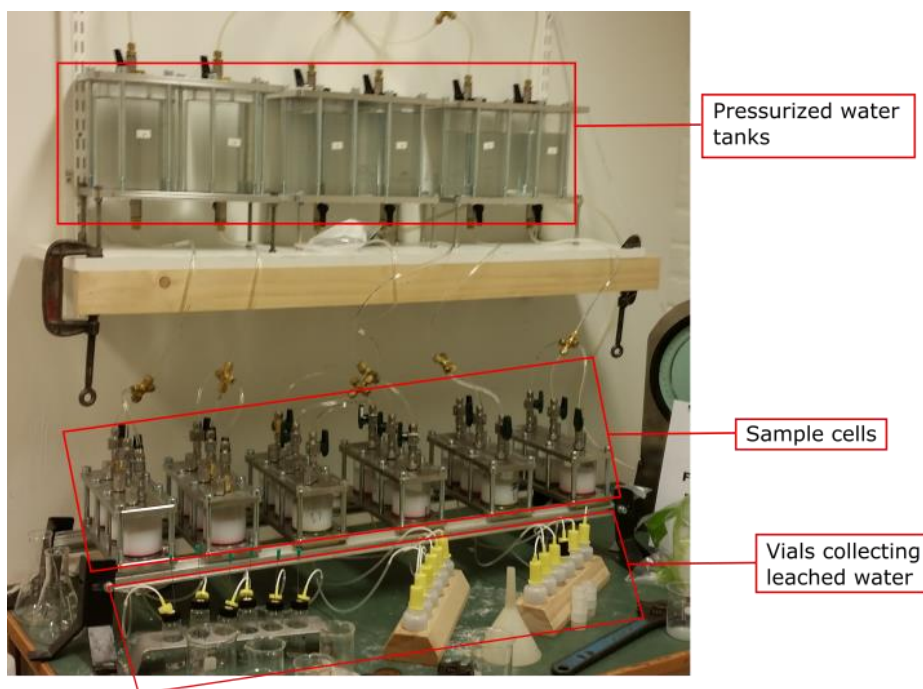


Figure 16: Complete sample setup with water tanks, sample cells, and sample vials.

Figure 16 above the sample cells the pressurized water tanks can be seen. These water tanks hold the water that is lead down to the sample cells. The water tanks are put under pressure to fascilitate the passage of water through the gels.

The water that passes through the gels will give data on what salts leave the gels and how much silica is dissolved. The data is collected by measuring the total concentration of elements by inductively coupled plasma on the water collected in the plastic vials. In addition to the ions concentration in the water the volume can also be measured by weighing the water in the vials. This will give an indication of how well the gels prevent water from passing through over time, that is, how the hydrodynamic conductivity of the gels varies over time. The main purpose of this equipment is thus to measure the degradation of silica gels dependent on the composition of the water that passes through, to measure the amount of water that passes through, to measure how much of the ions used to create the gels (accelerator ions) leave the gels and to measure how ions that enter the gels with the water behave in the gels.

3.7.2. Test setup

In total and as can be seen in Figure 15, six setups were constructed. These were named A to F. Setup A and B was the first two setups to be completed and were therefore the setups used in the initial tests. These tests were started by moulding 100 mL of gel into each of the sample cells. To hold the silica sol in the cells during the gelling process the 3D printed filters were pre-treated with silica sol by allowing it to gel in the filter. The gel times were always kept to about 20 minutes and for setup A 2M NaCl and setup B 2M KCl was used as accelerator. This resulted in setup A having 81.4 mL of silica sol and 18.6 mL of NaCl solution per sample cell while for setup B corresponding values are 88.6 mL and 11.4 mL. These values show the relative effectiveness of the NaCl and KCl accelerators since more NaCl is needed to achieve the gel time of 20 min. For both setups A and B the water used in the water tanks was pure Milli-Q water.

Once the gels were in place they were left for 24 hours with a small amount of water on top to prevent drying. After this time all the air was removed from the system and the pressure on the water tanks of 9810 Pa was put on. This lead to water slowly passing through the gels

and ending up in the sample vials. At the start of the tests one vial per sample cell was collected once every week. As the tests preceded this was reduced to one vial per month.

Once setup A and B had proved that the test design worked as intended and construction of setups C-F had been completed these four setups were started. In these later setups the pH and ion content of the leaching solution was varied to simulate different scenarios, see Table 2.

Table 2: Show the different setups, accelerator used to create the gels, the total test time for the different setups as well as ion compositions and pH of the leaching water (water in water tanks).

Setup	Accelerator	Ion content of the leaching solution (mM)	pH of leaching solution	Test duration (days)
A	NaCl	None	6-7	488
B	KCl	None	6-7	488
C	NaCl	Na: ~10	12 ± 0.5	221
D	KCl	Na: ~10	12 ± 0.5	221
E	KCl	Na ⁺ : 86 Ca ²⁺ : 34 Mg ²⁺ : 5 Si: 0.18	8-9	221
F	KCl	Na ⁺ : ~108 Ca ²⁺ : 34 Mg ²⁺ : 5 Si: 0.18	12 ± 0.5	221

Setup C and D was used to test the effect of high pH on the stability of the silica sols. Often sols are used as grouting material in combination with cement which leads to a basic environment of high pH levels. It is well known that the solubility of amorphous silica increases rapidly at pH above 10 due to formation of silicic acid (72). These setups will thus give us an insight in how the gels cope with high pH levels.

Setups E and F simulate the presence of a typical Swedish groundwater. It contains a number of salts, the cation of which can be seen in Table 2. Setup E has the “natural” pH of the groundwater while setup F has been adjusted to pH 12 to account for presence of cement.

The pH of setups C, D, and F was monitored monthly to make sure that the pH was kept around 12. Since air was used to generate the pressure in the water containers the presence

of CO₂ in the air may lead to formation of H₂CO₃ which will reduce the pH. To prevent this, the pH was readjusted using appropriate amounts of NaOH every month.

3.8. Inductively coupled plasma – atomic emission spectroscopy

The analytical method of inductively coupled plasma – atomic emission spectroscopy (ICP-AES) is an established method of measuring the concentration of elements. The sample is introduced in the form of an aerosol into a plasma burner with a temperature of 6000 – 10 000 K (83). At this temperature all molecules disintegrate and only free atoms will be present in the plasma. Some of these free atoms will be excited by the extensive heat meaning that some electrons in these atoms will jump up into a higher energy level. Electrons do not stay long in the excited state and as they fall back to the original energy level they will emit photons. The wavelength of the photons is specific for the element emitting them and can be measured. The method is very sensitive and ICP-AES has detection limits of 3-50 ng/g.

In this thesis the ICP-AES is used to measure the concentrations of Na, K, Mg, Ca, and Si in the samples produced from the silica gel long term stability tests described in part 3.7. Since the samples contained high salt concentrations all samples were diluted 1000 times with 0.5M HNO₃. Three standards were run before each measurement session to assure accuracy.

4. Results and discussion

The results presented are based on the papers I-VI included in this thesis. Discussion starts with presenting the interactions of ions with the silica surface and the impact this has on the stability of silica sols and on the formation of gels. It shortly touches on how temperature and particle size affect aggregation. It then moves on to tests performed for determining the long term stability of silica gels. This part will “gradually zoom out” as discussion moves from the atomic interactions at the silica interface to the behaviour of the silica gels as a material.

4.1. Ion-silica interaction

As mentioned in the introduction, the Hofmeister series for monovalent ions is well established for silica surface (direct Hofmeister series $\text{Li}^+ < \text{Na}^+ < \text{K}^+ < \text{Rb}^+ < \text{Cs}^+$) the effects of anions (co-ions) are not well established, especially for ions common in ground water. Furthermore, for divalent ions a hitherto unexplained shift in the Hofmeister series is seen for magnesium where Mg^{2+} shows stronger interaction with the negatively charged silica than Ca^{2+} . This goes against the structure maker/structure breaker as well as the ease of polarizability of ions arguments which are usually used to explain the behaviour of the monovalent cations. Clearly some other phenomenon is at work for the Mg^{2+} ion.

4.1.1. Co-ion effects

The effect of co-ions on the stability and surface chemistry of colloids has been previously noted but not fully explained (84-86). In Figure 17 the impact on gel time for colloidal silica Ludox TM-40 in a number of sodium salts with different anions is shown. As can be seen there is a clear difference between the different salts in their ability to induce aggregation. The strongest difference is observed between NaCl and Na_2SO_4 which is in tandem with data reported by Huang *et al* (67). Note that the lacking results for concentration of 0.235 M Na_2SO_4 is due to the fact that no gelling was observed at this concentration within 24h. The time within which the gels are formed is dependent on the number of cations present at the silica solution/interface. Figure 17 clearly shows that the co-ions are able to somehow affect this in the following order $\text{Cl}^- < \text{ClO}_4^- < \text{ClO}_3^- < \text{NO}_3^- < \text{SO}_4^{2-}$. The gel time results show that the effect on gel time is significant and tests performed with K^+ as cation for Cl^- , NO_3^- , and SO_4^- show the same trend, see paper II.

The results generated by the gel time tests are strengthened by the results from potentiometric titrations on the silica nanoparticles in presence of a number of salts. From the titrations the surface charge density is calculated and data for some salts is shown in Figure 18. While the impact on surface charge density of the different co-ions is not as pronounced as for the gel time tests, the trends are similar. The salts with Cl^- anions show the highest surface charge densities which indicate that Na^+/K^+ interact strongly with negatively charged silica. This explanation is physically sound because it is well established that when counter ions are strongly interacting with the charged groups on oxide surfaces they facilitate the deprotonation resulting in an increase in surface charge density and in case of silica the surface becomes more negative. On the other hand sodium and potassium salts with NO_3^- and SO_4^- as anions show lower surface charge densities which indicates lower concentrations of Na^+/K^+ at the silica/solution interface. This is consistent with the gel time tests where in salts with these anions showed longer gel times compared to Cl^- containing salts.

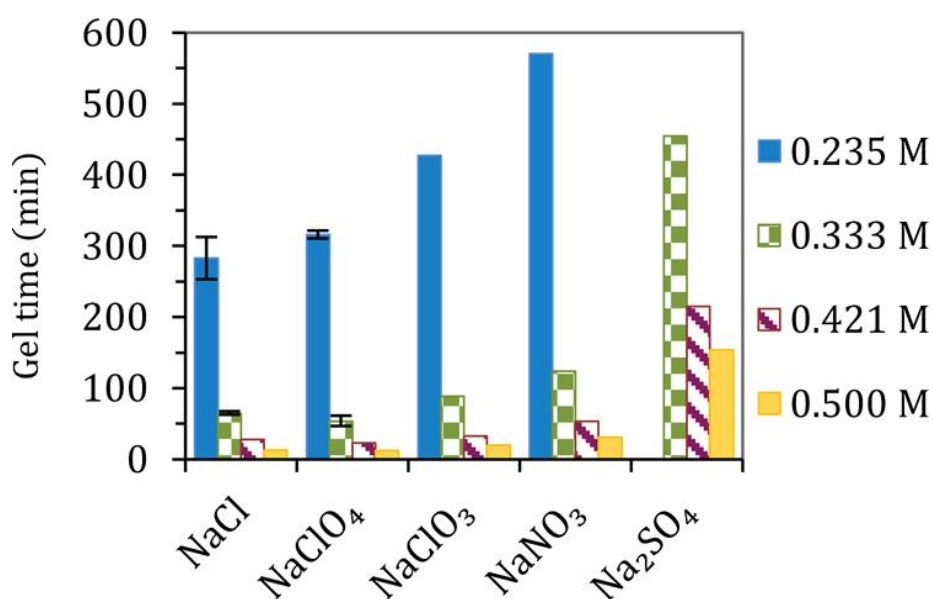


Figure 17: Shows gel times for a number of salts where the anion and salt concentration varies (87). Concentrations are shown for the cat-ions of the salts.

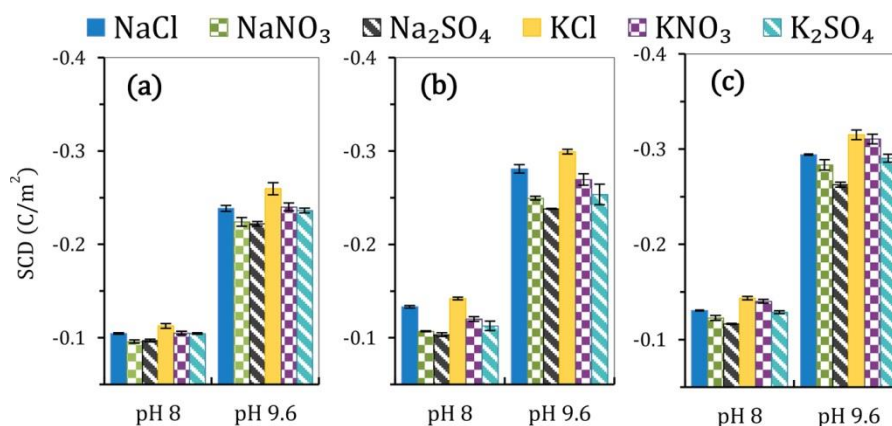


Figure 18: Surface charge density for silica nanoparticles at pH 8 and 9.6 in presence of a number of salts at different concentrations: (a) 0.05M, (b) 0.1M, and (c) 0.2M.

We can thus conclude from the results presented in Figure 17 and 18 that the type of anion in salts does affect the interactions of cations with the silica surface but an interesting question is why this occurs.

These results can be rationalized by observing the trends in the activity coefficients of these ions in solution, see Figure 19 and 20. The lower the activity coefficients are the less dissociated are the ions in the solution. Ions in salts such as Na_2SO_4 and K_2SO_4 due to their low activity coefficients form ion pairs in solution. This means that when ions are paired in solution there will be less free cations which will interact with the silica surface and thereby the effective concentration of cations at the silica/solution interface will be reduced. Such reduction of cations at the silica solution interface leads to longer gel times/lower surface charge densities as shown by results presented in Figure 17 and 18. The trends in the activity coefficients of different salts (Figure 19 and 20) closely follow the trends observed in gel times and surface charge densities shown in Figure 17 and 18, respectively. One of the reasons for the formation of ion pairs is the degree of polarizability of the anion. For example the sulphate anion is more polarizable than the nitrate which in turn is more polarizable than chloride. This means that sulphate can more readily form an induced dipole which will increase its interactions with cations compared to nitrate and chloride. Further discussion regarding this phenomenon can be found in paper II.

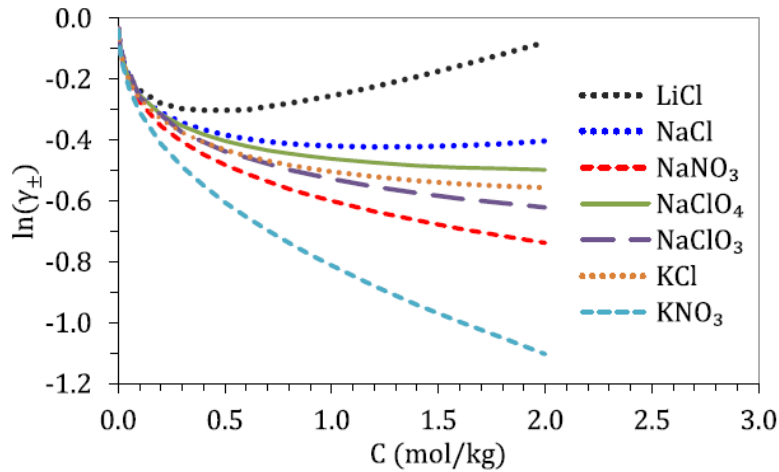


Figure 19: The natural logarithm of mean ionic activity coefficients for a number of aqueous electrolyte solutions plotted against the cat-ion concentration. The data was obtained from experimental values provided by Hamer and Wu (88) and Goldberg (89).

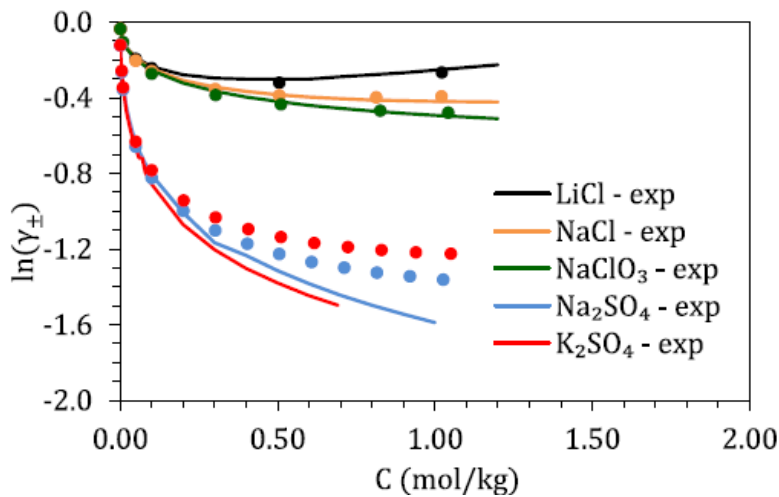


Figure 20: Graph showing the mean ionic activity coefficients for experimental data (solid lines) and calculated by MC simulations (round markers). Data produced by Hamer and Wu (88) and Goldberg (89). Note the large decrease in activity for the sulphate salts.

4.1.2 Divalent ions

There are many similarities between the monovalent ion series of alkali metals and the divalent ion series of the alkaline earth metals. For both series the polarizability of the ions increases with ion size as we move down in the periodic table (90). This means that larger ions should be able to interact more strongly with the silica surface since they will be easily polarizable as they approach the silica surface. The ions in both series also show increased hydration the smaller the crystallographic ion size is (62, 91). The increased hydration has traditionally been seen as a hindrance in the ions ability to interact with the silica surface.

One clear difference between the two series is the valency of the ions. The divalent ions are, due to their valency and in accordance with the Schulze Hardy law, more efficient in the destabilization of silica nanoparticles. However, comparing the two divalent ions such as Mg^{2+} and Ca^{2+} we expect that Mg^{2+} due to smaller crystallographic size, less polarizability, and stronger hydration to interact relatively weaker with negatively charged silica surfaces compared to Ca^{2+} .

In Figure 21 the observed changes in gel times for Mg^{2+} and Ca^{2+} salts at different pH values are shown. At pH values 9 and above the gel times in magnesium salts are much shorter than

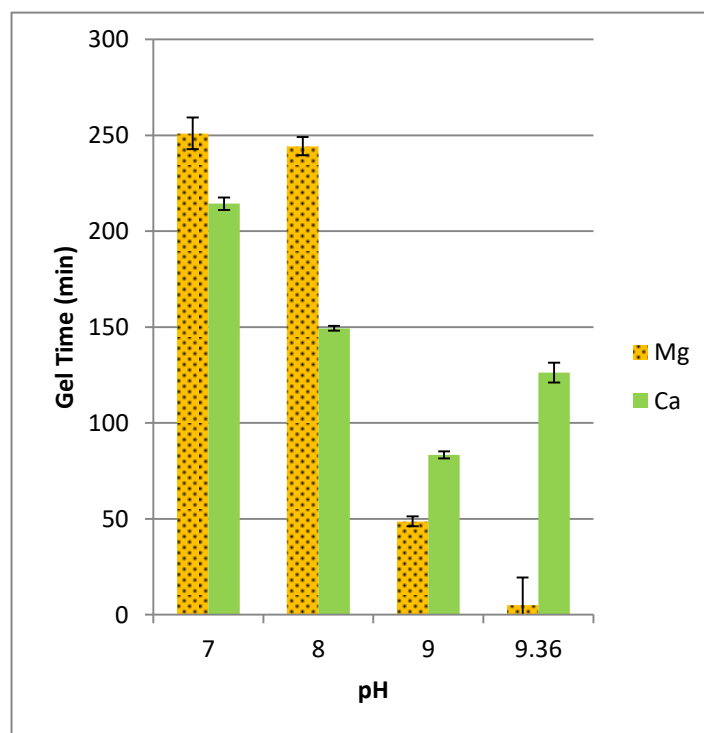


Figure 21: Gel times for $MgCl_2$ and $CaCl_2$ for a range of pH levels. The pH 9.36 is the original pH of the silica sol. A shift in gel time can be observed for Mg as its gel time increases above that of Ca when the pH is reduced below 9.

in calcium salts which means a reversal of the Hofmeister series. More surprisingly there is a shift in gel time between pH 8 and 9. Below pH 9, Ca^{2+} is the more effective destabilizer and thus interacts stronger with the silica surface than Mg^{2+} which is in accordance with the direct Hofmeister series. This shift occurs at the pH (8,5-9,9) values which correlate with the pKa (8,5) of isolated silanol groups on the silica surfaces and 81-85% of such groups are deprotonated. The strongly charged silica nanoparticles will acquire a strong hydration layer. On the other side when strongly hydrated Mg^{2+} ions with polarized water approach the surface they will interact strongly. This situation is similar to what Colin has put forward the

idea of enhanced interaction between the species of similar water structures (92). The change in pH will affect the distribution of Si-O⁻ groups on the surface. As pH becomes lower than 8.5 the number of charged groups will start to decrease and there will be mixture of Si-O⁻ and Si-OH groups. At pH values > 9 the Mg²⁺ ions having strongly polarized water i.e., hydrated water molecules will have more positively charged hydrogens than the water surrounding Ca²⁺ (Figure 22). The water around Mg²⁺ will thus interact more strongly with highly negatively charged hydrated silica. However, at pH values less than 8.5 due to the presence of less charged groups such preferential

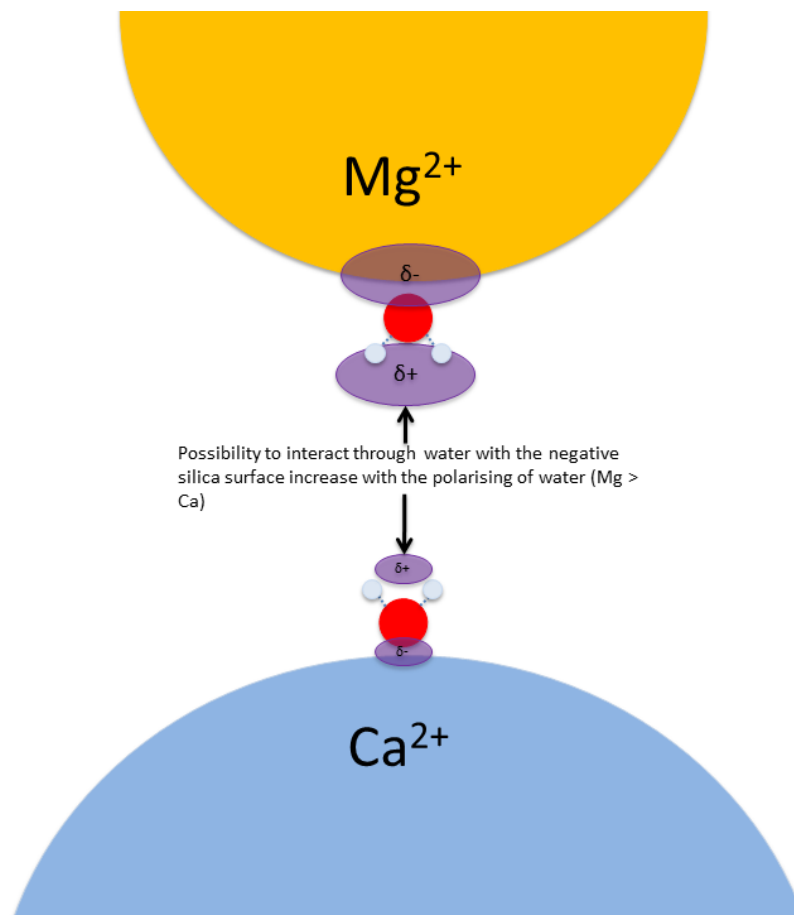


Figure 22: Conceptual figure of the polarization of water that occurs around Mg²⁺ and Ca²⁺. The polarization degree is shown by the size of the δ+ and δ- areas.

interaction of Mg²⁺ with the weakly charged silica will not prevail. In such situation the relatively easily polarizable Ca²⁺ ions will preferentially interact with the silica surfaces.

A further question arises, why do we not see such pH dependent shift for Li⁺ as we have seen for Mg²⁺? The proposed explanation is based on the strong hydration of small ions such as Li⁺ and Mg²⁺ as well as of silica nanoparticles. The small size combined with the high charge

density of the Mg^{2+} ion mean that it should be able to polarize hydrating water molecules to a higher extent than Li^+ ion. This means water molecules hydrating Li^+ do not have as positive charge displacement on hydrogen as does Mg^{2+} . All of these ions most probably will keep their hydrating water when interacting with the silica surface and will thus interact with the silica through the water molecules. The ability to polarize water, see Figure 22, and thus form a water layer in which hydrogens are relatively more positive will thus affect the ability of these ions to interact with the silica. As we continue down the periodic table the ions will increase in size and they will start to lose their structured water layer and become the so called structure breaker ions. These big ions are not dependent on the polarization of water to interact with the silica surface but can interact directly with the surface due to their high polarizability or in other words dispersion interactions with the surface.

This explains why for example Li^+ interacts weaker than Cs^+ . Further strength to this argument is added when we compare the number of water molecules hydrating the Mg^{2+}

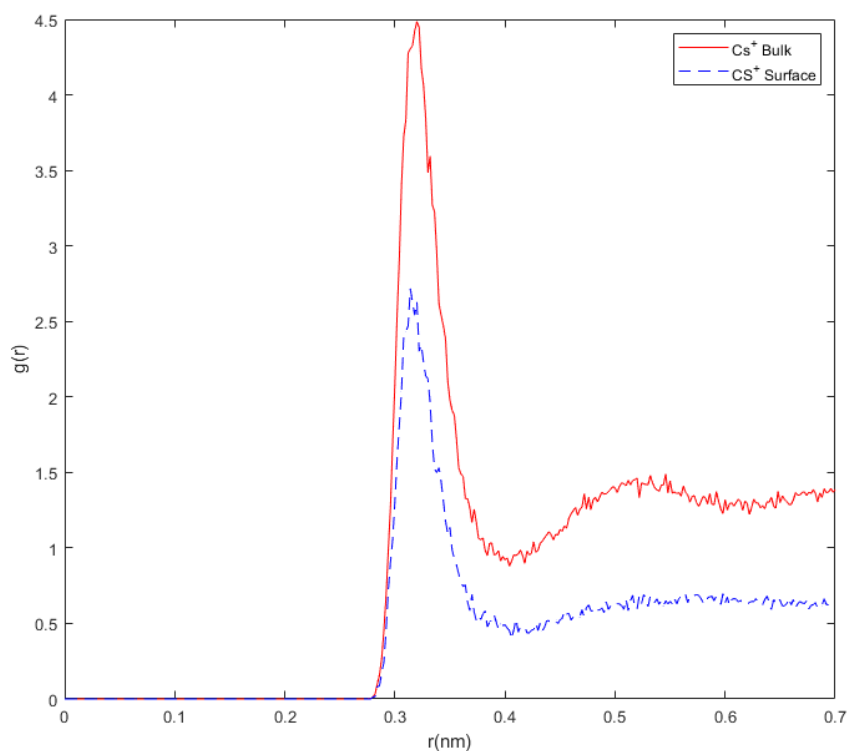


Figure 23: Radial distribution of water molecules surrounding the Cs⁺ ions in the simulation cell. Cs Single refers to the average distribution in the cell and Cs Surface to the distribution at the silica surface.

and Cs^+ ions. In Figure 23 the radial water distribution, taken from MD simulation for Cs^+ ions is shown. When the ions approach the silica surface we see a drop in the average number of water molecules hydrating the Cs^+ ions. This is clear evidence pointing towards inner sphere adsorption of the Cs^+ ions. A comparison of hydration in bulk and near the surface for Mg^{2+} is given in Figure 24. As can be seen there is no difference between the Mg^{2+} ions for the whole system and the Mg^{2+} ions at the surface. This means that Mg^{2+} does not lose its hydrating water molecules and must therefore interact with the silica surface through the

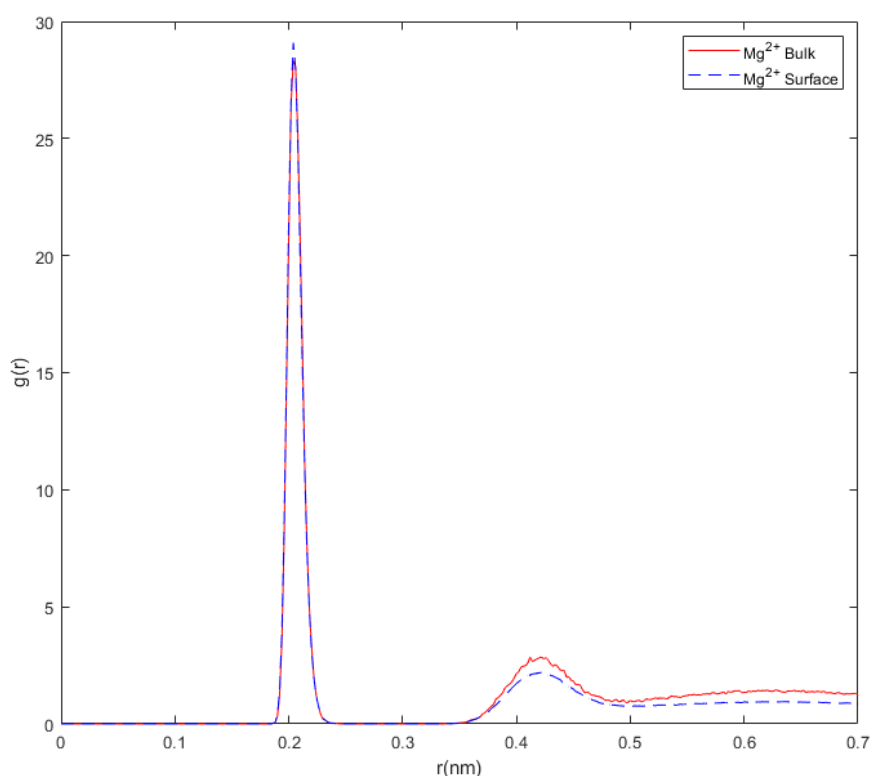


Figure 24: Radial distribution of water molecules surrounding the Mg^{2+} ions in the simulation cell. Mg^{2+} Single refers to the average distribution in the cell and Mg^{2+} Surface to the distribution at the silica surface.

water molecules.

To summarize this part it should be said that there are thus two modes of interaction. These have been called outer sphere and inner sphere complexes and Li^+ , Mg^{2+} , and Ca^{2+} are thus interacting through typical outer sphere complexes i.e., interact with the silica surface through water molecules. K^+ and Ca^{2+} as well as the large divalent ions such as Ba^{2+} interact

through typical inner sphere complexes that they interact directly with the surface. Na^+ is something in-between these two since it has a structured water layer but this layer is limited in size. Whether Sr^{2+} is also an “in-between” ion is currently unknown.

4.1.3. Mixed salts

Silica nanoparticles produced in industry are stabilized by simple salts such as Na_2O but research on using the silica in natural systems should be done in complex solutions. Major part of research on silica has been focused on single ionic systems with one cation and one corresponding anion (58, 60, 65, 93-99). In industrial environments it is not uncommon that mixtures of many ions are present. The behaviour of ions in solutions containing different ion types is therefore of interest. In this part, results regarding the gel times in salt mixtures where two salts with two different cations but the same anion are discussed. Since only the cations are different this will give insight into whether there is an interaction hierarchy for these ions at the silica surface. In Figure 25 results for gel time tests in two mixtures of monovalent ions are shown. In these tests the cation concentration has been kept constant at 0.33M with one cation gradually replacing the other. On the x-axis only the Li^+ concentration is shown and 0M Li^+ corresponds to 0.33M Na^+ or K^+ concentration. As can be

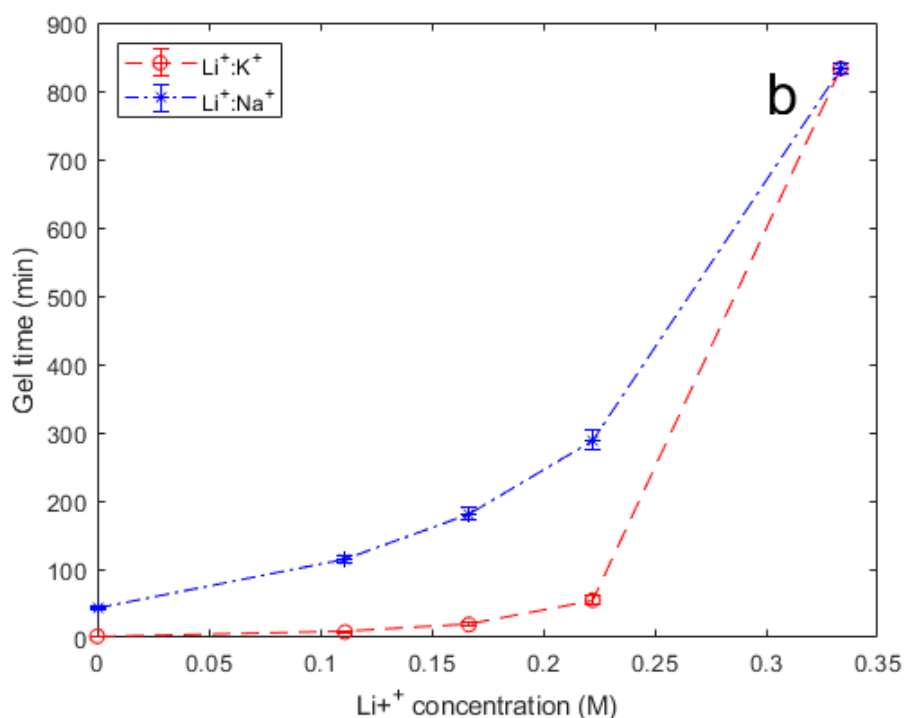


Figure 25: Results for gel time tests where Na^+/K^+ ions are gradually replaced by Li^+ ions. Cation concentrations are kept constant at 0.33M and the $\text{Li}^+ : \text{Na}^+/\text{K}^+$ concentrations correspond to 0.00 : 0.33, 0.11 : 0.22, 0.17 : 0.17, 0.22 : 0.11, 0.33 : 0.00 (M).

seen the gel times do not show linear correlation when Li^+ successively replaces the Na^+ or K^+ ions. The interpretation of this nonlinear behaviour is that the Li^+ ions are not able to completely displace the Na^+ or K^+ ions at the silica solution interface to an equal amount corresponding to their concentrations. For example a 20% increase in Li^+ concentration does not lead to 20% decrease of Na^+ concentration in the interface. If that was the case the gel times should have been increased linearly. This behaviour is due to the ability of Na^+ and K^+ to interact stronger with the silica surface than Li^+ and is in agreement with the Hofmeister series. However, the gelling times in the mixture of Li^+ and Na^+ looks more linear than in the K^+ and Li^+ mixture. Li^+ and Na^+ are next to each other in the Hofmeister series and both are classified as structure maker ions and it is thus not surprising that Li^+ can more easily replace Na^+ at the interface than K^+ . In Figure 26 results of gel time tests in the mixtures of divalent and monovalent ions are shown. The concentration of divalent ions has been kept approximately constant while the concentration of monovalent ions has been successively increased. This means two things; the driving force to displace divalent ions at the silica

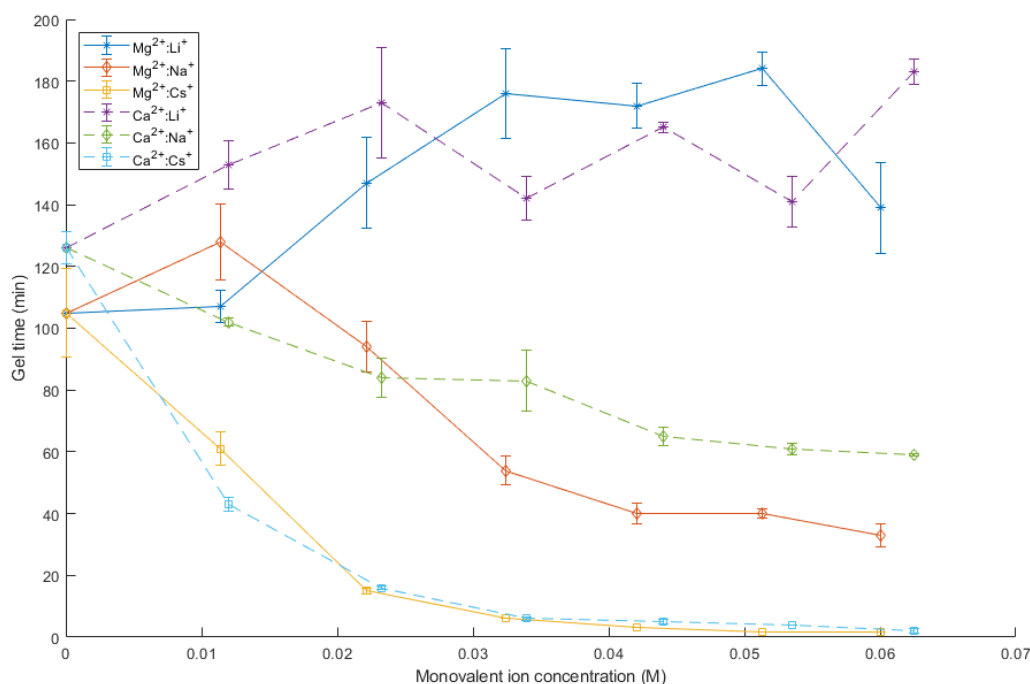


Figure 26: Shows mixtures MgCl_2 and CaCl_2 with a number of monovalent ions where the divalent ion concentration has been kept approximately constant at around 0.0235 M - 0.0200 M and 0.0296 M - 0.0250 M respectively; only the concentration of monovalent ion changes significantly.

solution interface should increase with monovalent ion concentration because the total ionic

strength of the solution increases as monovalent ions concentration increases. It is not surprising that most mixtures show decrease in gel time as the ionic strength increases since an increase in the number of ions at interface leads to enhanced screening. However, a collection of results for Mg^{2+}/Li^+ , Ca^{2+}/Li^+ , and to some part the Mg^{2+}/Na^+ salt mixtures show increase in gel time for the first few increments of monovalent ion concentration. This is clear evidence that even though the divalent ions interact strongly with the silica surface and are thus not displaced proportionally to monovalent ions, some exchange still occurs. Some Li^+ ions will thus remove some Mg^{2+} from the silica surface and since Li^+ is not as effective in screening the electrostatic repulsion forces we see longer gel times. Further discussion regarding mixed ion systems can be found in paper III.

4.2. Development of PEEK capillary for electrospray

This part deals with the development of a PEEK capillary for electrospray which can be used in the ES-SMPS method. This is treated in short since it is the result of a “side project” that

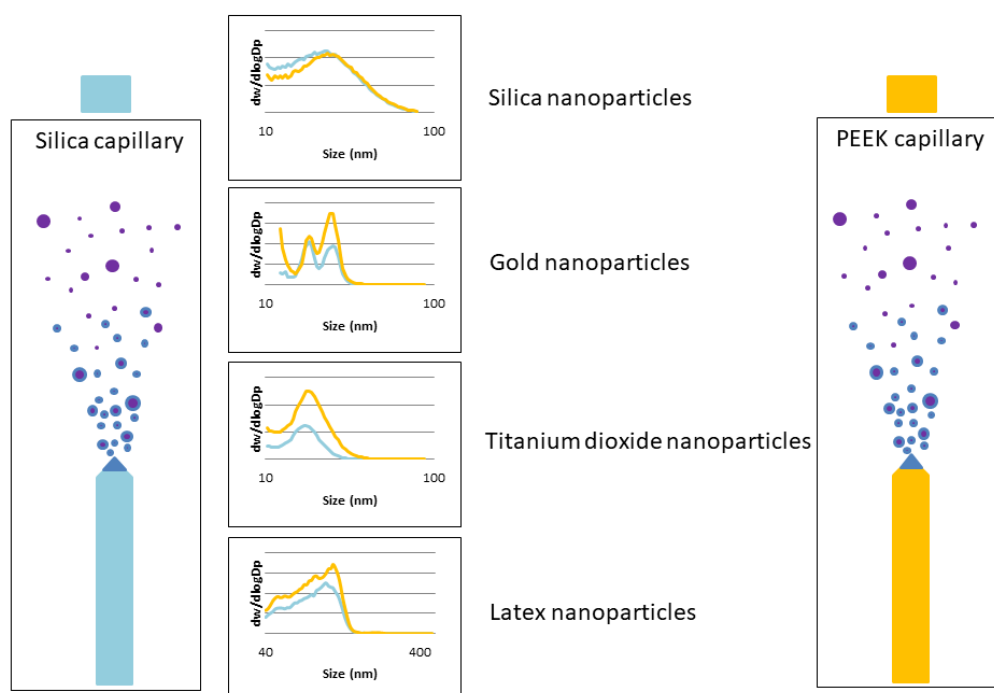


Figure 27: Summary of data comparing the standard silica capillary (blue) with the plastic PEEK capillary (orange).

lead to the publication of paper IV. The method ES-SMPS is used quite extensively in part 4.3.

Typically for electrosprays used to spray particles is that a silica capillary is used. This capillary will carry a charge similar to that of silica nanoparticle as described by equation 4. The capillary surface is thus negatively charged at most pH values and this limits the pH range at which certain particles can be sprayed. Positively charged particles passing through a negatively charged capillary will be attracted to the capillary surface and will result in clogging of the capillary. To prevent this clogging a PEEK capillary was adapted for use in electro spray. The advantage of the PEEK capillary is the lack of surface charge meaning that any type of particle can be sprayed regardless of the particle surface charge. We tested silica, gold, latex, and titanium particles and compared results from the use of the standard silica capillary with results from the PEEK capillary. A comparison of results is given in Figure 27. We have not observed any major differences in the particle size distribution between the silica capillary and the PEEK capillary. The PEEK capillary produced more particles than did the silica capillary for all particle types except for silica nanoparticles. The PEEK capillary thus performed satisfactorily. Further discussion about these results can be found in Paper IV.

4.3. Particle aggregation – Temperature and particle size effects

In this part results from gelling of sols at three different temperatures (10°C, 20°C, and 30°C) will be discussed. The sols tested were CS30-236, CS40-222, and CS40-213 with an average size of 16.82 nm, 21.67 nm, and 33.78 nm, respectively. Whenever particle size is referred to in this part the reference is to the average number mobility particle size which has been measured using ES-SMPS. The average number mobility particle size is the number average of the aerodynamic diameter since the ES-SMPS separates charged particles based on their aerodynamics size in an electric field.

In Figure 28 data collected from gel time tests using these three sols at the three temperatures is shown. Aggregation was induced by adding 2.48 mL of 2M NaCl solution into 15 mL sol giving a constant ion concentration of 0.28M for all tests. Particle content was kept constant around 30 wt%. It is clear that the smaller particles show the shortest gel times and

thus the fastest particle aggregation. Furthermore, increase in temperature reduces the gel times for all sols but the trends are clearer for the largest particles of CS40-213. Gel time thus decrease with particle size according to $16.82 \text{ nm} < 21.67 \text{ nm} < 33.78 \text{ nm}$ and with temperature according to $30^\circ\text{C} < 20^\circ\text{C} < 10^\circ\text{C}$. Both of these rankings are connected to the Brownian motion of the particles since at higher temperatures and smaller particle size the motion increases. This leads to higher collision rates which at constant salt concentration facilitate faster gel build-up.

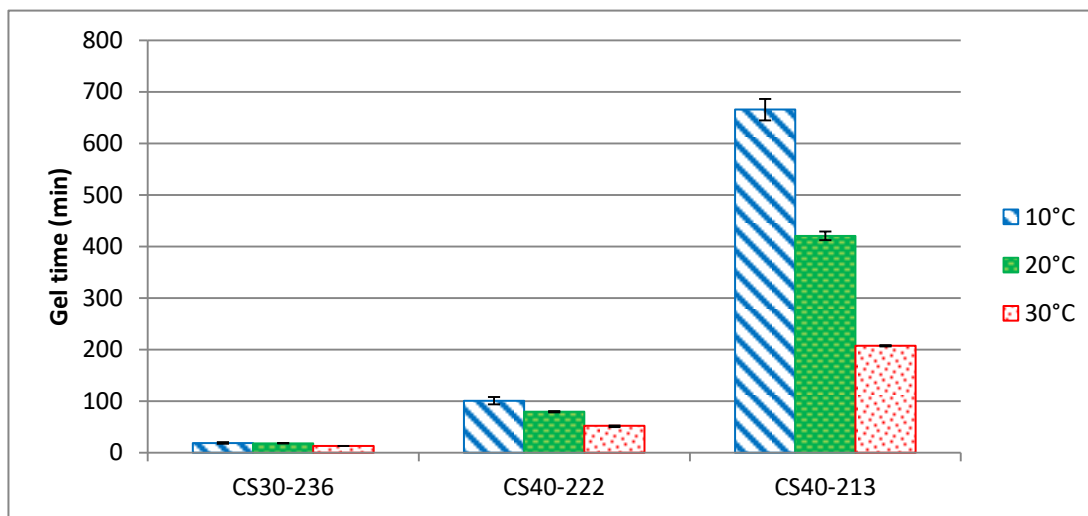


Figure 28: Gel times for the three different silica sols at 10, 20, and 30 °C. The trends are clear in that higher temperature results in shorter gel times.

In Figure 29 the complex viscosity development for the three sols at the three temperatures is presented. These tests confirm the trends seen in the gel tests that increased temperature and decreased particle size lead to faster gelling. The rheological tests also give information on the nature of the gelling procedure. All sols show an exponential increase of the complex viscosity. This means that the sols remain at low viscosity for a long time until close to the gel point where the viscosity increases sharply. We would expect that this behaviour corresponds to a very rapid formation of the continuous gel network from small aggregates. There is thus not a gradual build-up of larger aggregates but the gel network is formed from rapid aggregation of smaller aggregates. Only CS40-213 at 10°C and 20°C show any kind of gradual build-up of viscosity but here also the build-up show an exponential nature.

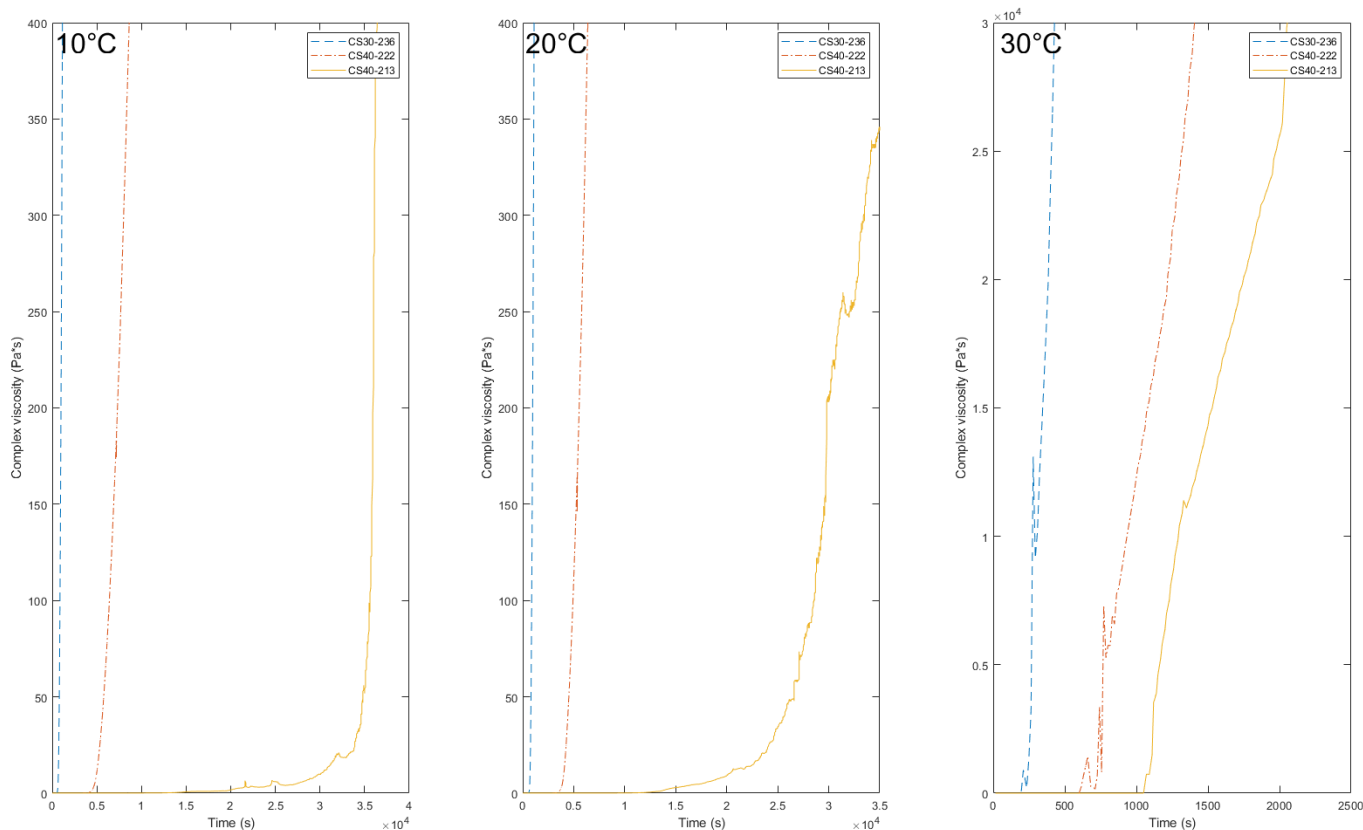


Figure 29: Complex viscosity development with time at the three temperatures for all three sols. As can be seen the complex viscosity development is sudden and rapid once the gel point is reached.

The ES-SMPS method was used to follow the aggregate formation of the three sols. Samples were collected from gelling at a specific temperature and percentages of the gel times shown in Figure 28. A distribution for each sol and temperature was thus generated at 0%, 25%, 50%, and 75% gelling. 100% gelling sample could not be collected since to be analysed by ES-SMPS the sample must be liquid and a collection of solid sample would mean breaking of the formed particle network. The results from these measurements are presented in the supporting material for Paper V.

From the ES-SMPS results it is possible to calculate the N_d values using equation 12. This gives us the average number of particles contained in an aggregate of average size. As time proceeds and aggregates grow the calculated N_d value will increase. In the calculation made in this thesis a d_f value of 2.1 is used which corresponds to RLCA aggregation. Using the values of N_d calculated for each percentage of gelling it is possible to extrapolate an N_d value to 100% gelling, that is average number of particles in an aggregate at the gel point. The results of the extrapolation for each sol and temperature can be seen in Figure 30. These N_d

values would seem to fluctuate around the value 3 particles/aggregate. Indeed if we calculate the average N_d from all the data shown in Figure 30 we get 3.01 ± 0.33 particles per aggregate. This value might seem low and is definitely nowhere near the size of the continuous gel network which contains a very large number of particles. However, this is an average value and thus points towards a large number of particles are not being included into the gel network even at the gel point. This is in agreement with a previous study on silica aggregation (59).

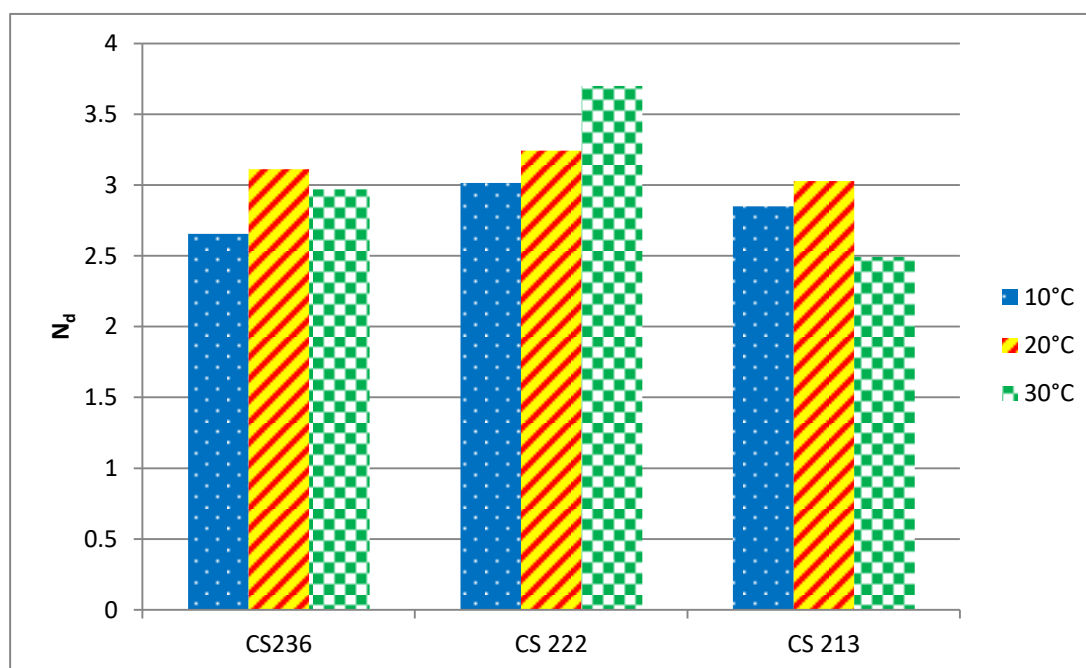


Figure 30: Average number of particles at the gel point calculated using equation 1 and extrapolated values from Tables 1-3. There does not seem to be any trend in the N_d values depending on average particle size or temperature with the N_d values fluctuating around 3.

Finally, using the gel times presented in Figure 28 an attempt was made to construct a mathematical formula which takes into account the average size of the silica nanoparticles and the temperature to generate and predict the gel time. The details of how this formula was derived can be found in Paper V but it basically contains a number of linear and polynomial fits. The end result is equation 18, where GT is the gel time in minutes, S is the number average particle size in nm, and T is the temperature in Kelvin. Equation 18 is thus derived from experimental data and is of empirical in nature.

$$GT = (-0.0734 * S^2 + 2.3831 * S - 19.6085)T + (22.494 * S^2 - 723.3304 * S + 5907.2) \quad (18)$$

Using equation 18 we predict the gel time over a span of particle size and temperatures the results of which are shown in Figure 31. It must be stated that equation 18 does not take into account the particle size distribution, the salt concentration, the pH, or the presence of organic molecules at the surface.

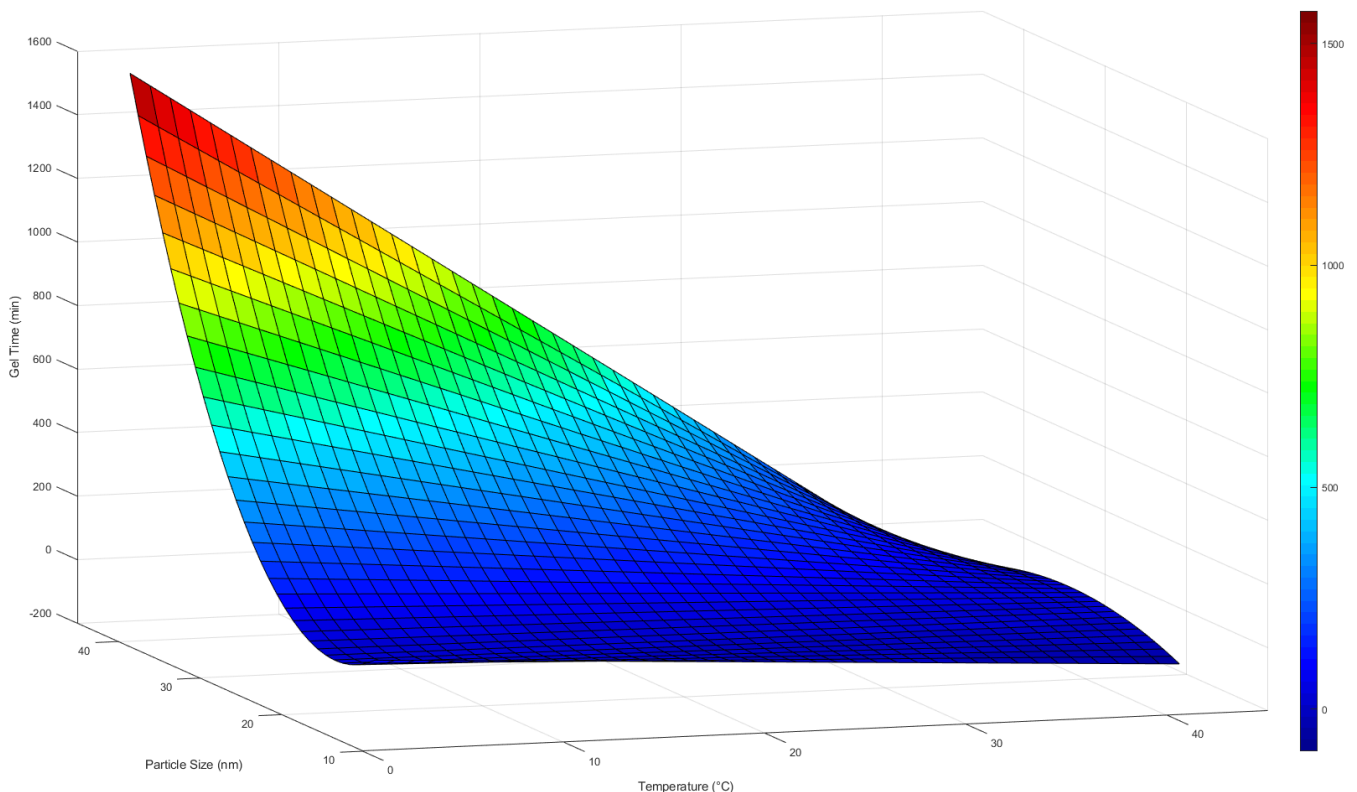


Figure 31: 3D plane plot for the prediction of gel times based on equation 2. The colour bar to the right helps with the interpretation of gel times and shows colours corresponding to gel time in minutes. Note that temperature is shown in °C while the calculations in Equation 10 have been made with the corresponding Kelvin units.

We tested the accuracy of equation 18 by measuring the gel times of two silica sols that were not included when the equation was derived, see table 3. The TM40 is a sol supplied by Grace and has an average particle size of 33.20 nm. When we compare the experimental gel time with the gel time predicted by equation 18 we see that it deviates quite severely with an underestimation of around 50%. We suspect that this might be due to the synthesis

method used for this specific sol which might lead to a different surface chemistry than of the CS-sols. For example, if TEOS has been used to produce the particles, organic molecules may still be present in the sol and lead to increased particle stability. For the CB17 sol equation 18 is more accurate with an underestimation of only 18%. Here equation 18 gives a hint at the magnitude of the gel time. The increased accuracy observed by CB17 compared to TM40 is probably due to the CB17 having the same producer (Nouryon) as the CS-sols and the synthesis procedure should therefore deviate minimally leading to similar surface chemistry.

Table 3: Experimental gel times for CB17 and TM40 sols at 30°C generated to compare with the theoretical gel times generated by equation 18.

Sol	Number average particle size (nm)	Temperature (°C)	Gel time Experimental (min)	Gel time from Equation 18 (min)
CS40-213	33.78	30	207.33 ± 1.25	209.74
TM40	33.20	30	418.00 ± 4.55	200.83
CB17	29.87	30	186.33 ± 10.37	152.81

4.4. Long term gel stability tests

As an ionic solution is introduced into silica sols aggregation commences and a gel is formed. The gel consists of a continuous particle network with large amount of water in it. If the gel is put under a water pressure, water will slowly flow through the gel. This flow can potentially result in loss of ions in the gels as well as dissolution of the particles in the gel network. In this part results from the long term gel stability tests are presented where waters of different ionic composition and pH are allowed to pass through gels made from mixing silica sol and 2M NaCl or 2M KCl solutions. Further details on the test setups are found in part 3.7.2.

In Figure 32 the Na⁺ concentrations from the leach water exiting the gels are shown. For setups A and C NaCl was used to form the gels and we therefore see large amounts of Na⁺ exiting the gels in the beginning of the tests. Setups B and D used KCl to form the gels and the Na⁺ ions exiting these gels are from the Na₂O used by the producer of the silica sols as stabilizer. The water entering setups E and F contained approximately 100 mM of Na⁺ ions and it is therefore not surprising that these setups hold constant exiting concentration of

about 100 mM. The gels generated by using K^+ salt show similar behaviours and more details can be found in paper VI.

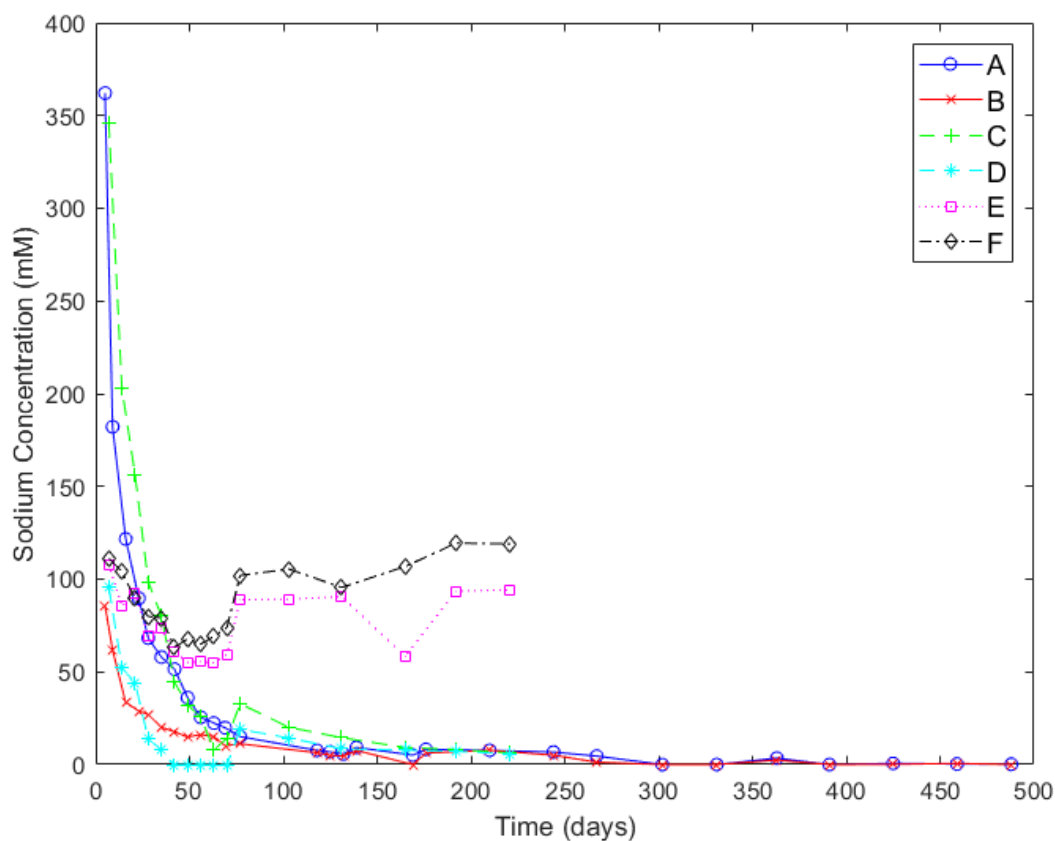


Figure 32: Concentrations of Na^+ in the leach water exiting the gels shown over time. Setups A and B shows high starting concentrations since NaCl was used to form these gels. B and D show presence of Na^+ due to the Na_2O used as stabilizer by the sol manufacturer. All setups show decrease in Na^+ exiting the gels over time with the exception of E and F where Na^+ is present in the water entering the gels.

Using the exiting amounts of Na^+ and K^+ from the gels, exiting volume of water from the gels and the knowledge about how much salt has been used to form the gels; it is possible to calculate the amount of K^+ or Na^+ that is left in the gels. In Figure 33 the results of these calculations are shown for setups A and B. It is clear that Na^+ leaves the gels to a higher extent than does K^+ . This is due to the stronger interactions between the silica surface and the K^+ cations, which is in accordance with the Hofmeister series. In setup B K^+ was used to form the gels and the Na^+ exiting the gels in setup B is thus from the stabilizer (Na_2O) of the sol. It is interesting to note that it follows the same behaviour of the much more numerous Na^+ ions in setup A (where Na^+ was used to form the gels). The implications of the results

shown in Figure 33 is that even though it is true that the network is formed at the gel time the loss of ions may affect the continued build-up of the gels and thus the strength development of the gels. This may result in weaker gels and this would be especially likely for Na^+ salt. In applications where the continued strength of the silica gels is of importance, such as in grouting operations, it is better to use ions for gelling which interact strongly with the silica surface such as K^+ .

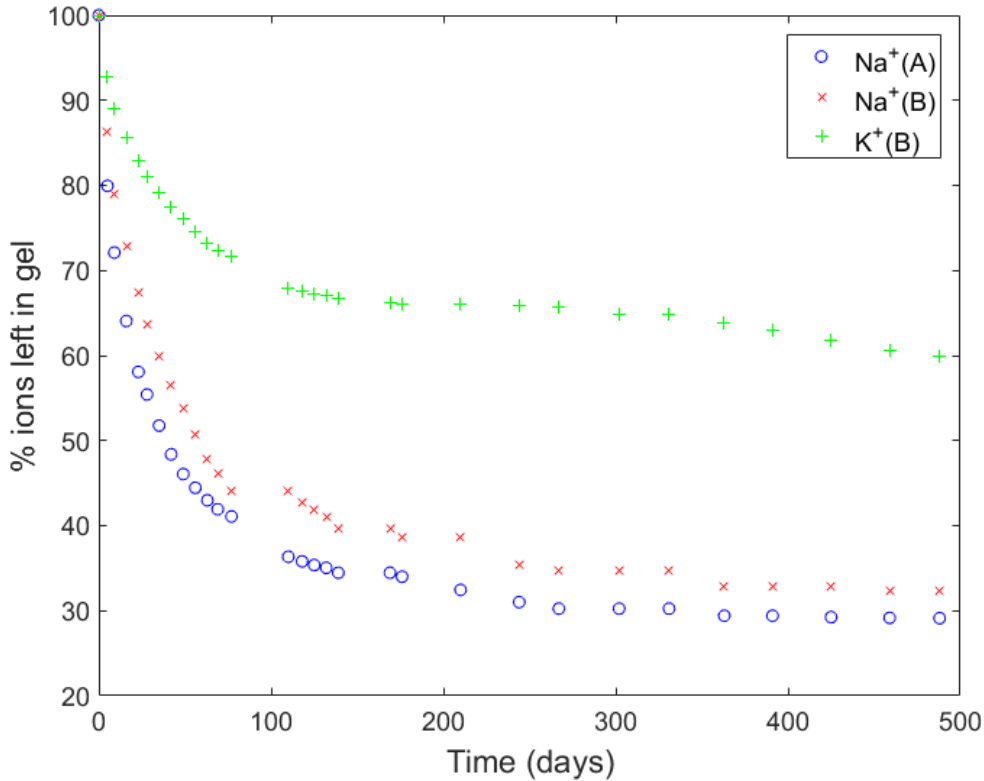


Figure 33: Percentages of Na^+ or K^+ left in the gels over time. These values are calculated using data shown in Figure 22 and corresponding data for K^+ . It is clear that K^+ remains in the gels to a larger extent than does Na^+ .

In Figure 34 the silicon concentration exiting the gels over time is given. Since silica solubility increase sharply above pH 10 (72) the expectations were that the setups with water having pH 12 entering the gels would lead to large amounts of gel dissolution and possibly gel failure. Overall the silicon content leaving the gels remains low for all tests. This is probably due to the fact that the gels will buffer the water that enters the gels to a pH around 9-10. This buffering capacity means that the solubility of silicon remains low. Setups C and D show a sharp increase in silicon content around 100 days. This is due to these setups having a pH of 12 for the water entering the gels. Setup C and D is thus pure mili-Q water with trace

amount of Na^+ since NaOH was used to adjust the pH. It is possible that after 100 days the gels ability to buffer has diminished somewhat leading to increased dissolution. However, setup F also had a pH of 12 but does not show the increased silicon content observed for C and D.

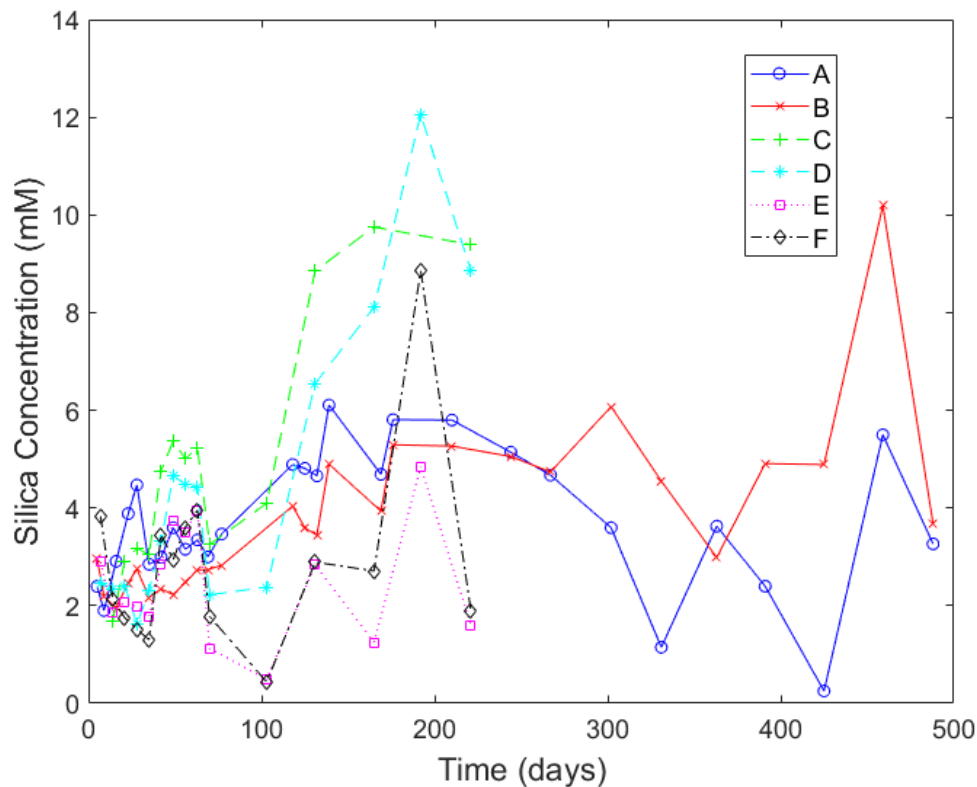


Figure 34: Silicon concentrations leaving the gels over time. Large fluctuations can be noted but C and D show the highest silicon content.

Another type of data extracted from the long term stability tests are the flow rate through the gels over time, see Figure 35. In general the gels where KCl was used show lower flow rates, e.g. when comparing A (NaCl) vs B (KCl) or C (NaCl) vs D (KCl). This is since more NaCl solution is needed to form the gels which lower the overall silica particle concentration in the NaCl gels. This leads to a lower density of the particles in the gel network which means that it is relatively easier for water to pass through the gel. The highest flow rates are observed for setups E and F. These setups have divalent ions, in this case Mg^{2+} and Ca^{2+} , entering the gels. These divalent ions will replace the monovalent ions at the silica interface and result in higher screening of the surface charge of the particle network. This screening

will limit the interaction of the surface with other ions which may result in higher flow rates through these gels. A more detailed description of this mechanism is given Paper VI.

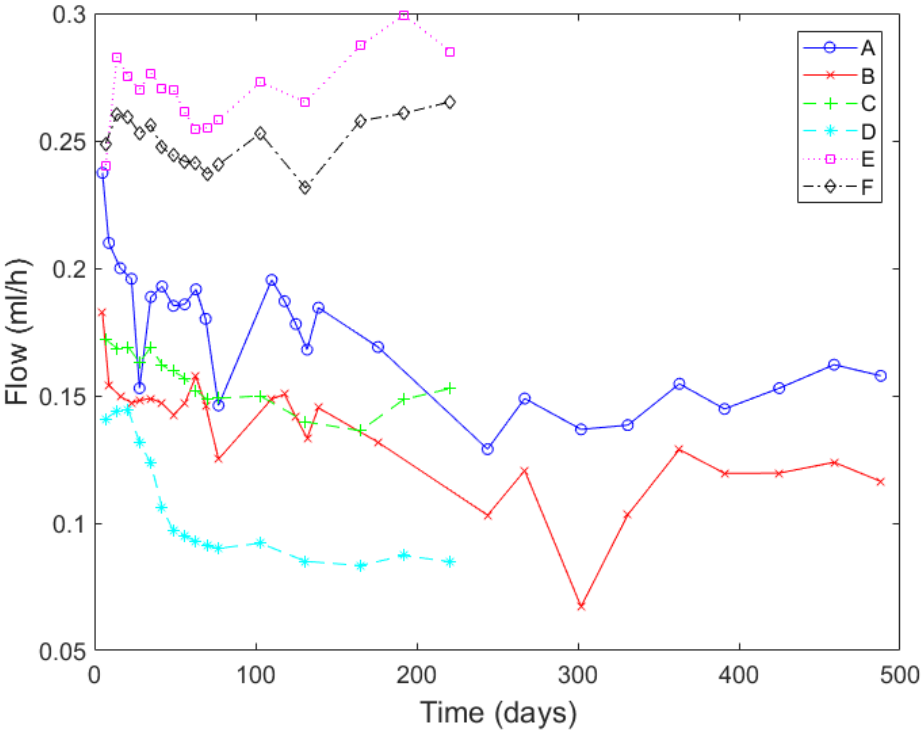


Figure 35: Flow rate through the gels over time. Overall the setups where KCl was used to form the gels show lower flow rates.

Using the data used for results shown in Figure 34 and 35 it is possible to estimate the total lifetime of the gels constituting the different setups. The estimations are based on linear extrapolations assuming that the values in Figure 34 and 35 do not change over time. The results of these calculations can be seen in Table 4. Setup D shows the longest gel lifetime of 395 years which is due to KCl used to form the gels leading to low flow rates and high silica particle content in the gels. The shortest gel lifetime, of 218 years, is shown by setup C which is due to high average silica content of water leaving the gels in combination with intermediate flow rates through the gels. Setups E and F, that represent real conditions experienced by gels used for grouting, show intermediate lifetimes with high flow rates but this is balanced by low silica concentrations of the waters leaving the gels. The conclusions drawn from these calculations of the gel lifetimes is that the salt used to form the gels have the largest effect, with more effective salts like KCl leading to longer lifetimes. The increased pH of the water that enters the gels did not show a significant reduction of the gel lifetime since the gels buffer the incoming water.

Table 4: Values for the dissolution of silica gels calculated from average flow rates and silica concentrations for the different setups.

% dissolved silica	Setup A years to dissolve	Setup B years to dissolve	Setup C years to dissolve	Setup D years to dissolve	Setup E years to dissolve	Setup F years to dissolve
10%	27	36	22	39	29	27
90%	240	321	196	355	263	242
100%	267	357	218	395	292	269

5. Conclusions

This thesis covers a rather broad range of phenomena present in silica sols and silica gels, ranging from ion interactions at the silica solution interface to the aggregation of silica nanoparticles and the behaviour of resultant silica gels. The conclusions will therefore be presented in the same order as the results have been presented in the thesis.

It was found that although the nature of the cation plays the prevalent role, the anions do affect the surface charge as well as the aggregation of silica nanoparticles. The effect of anions was present in both Na^+ and K^+ salts and the ranking follows $\text{Cl}^- \approx \text{ClO}_4^- < \text{ClO}_3^- < \text{NO}_3^- < \text{SO}_4^{2-}$. Chloride showed the fastest gel times and highest surface charge densities while sulphate showed the slowest gel time and lowest surface charge density. A plausible explanation of these differences in gel time and surface charge has been put forward, which is due to the ion pair formation as exhibited in the activity coefficients of the different salt solutions in which the gel time increases. Sulphates show the lowest activity coefficients thus indicating the formation of ion pairs and this will limit the cation concentration that can adsorb at the solution-silica interface. The activities coefficients of Na^+ and K^+ salts follow the ranking of anions as given above.

Divalent ions were shown to pass through a shift in the Hofmeister series between pH 8-9. This is due to the hydration of small ions and a shift in the nature of the silica surface since above pH 8 the silica carries a significant negative charge. This negative charge makes it easier for highly hydrated ions such as Mg^{2+} to interact with the surface through the ions hydration layer. Below pH 8 the silica loses much of its surface charge and such interactions are no longer as favourable.

Gel time tests in salt mixtures with two different monovalent cations showed that the exchange of cations in the silica solution interface does not linearly follow the respective concentrations of the ions. Ions higher up in the Hofmeister ranking (stronger interaction with silica surface) will remain in the silica solution interface to a higher extent even if their bulk concentration is lowered. There thus exists a hierarchy in the interaction of ions with the silica surface which is the same as the normal Hofmeister series. The shift in Hofmeister series observed for divalent ions is also present when observing the behaviour of mixed ionic solutions.

When silica nanoparticles form gels smaller particles will reach the gel point faster than larger particles. If the temperature is increased the gel point is reached faster. Both these effects are due to increased Brownian motion of small particles and higher temperatures. This leads to more impacts between particles which leads to faster aggregate formation and thus faster gelling. Rheometer tests indicate that the formation of a continuous gel network is very fast when the gel point is being approached. The average number of particles/aggregate at gelling is around 3 indicating that a large number of particles still exist as single particles at the gel point.

The long term stability tests of silica gel gave two main results. The first is that the accelerator ions used to create the gels do not stay in the gels when a water pressure is applied. The fraction leaving is dependent on the ion type used as an accelerator with K^+ staying to a larger extent than Na^+ . The second is that the total hydraulic conductivity is dependent on the amount of silica present in the gels. K^+ is a more effective accelerator than Na^+ allowing for more silica particles in the gels, resulting in lower hydraulic conductivity. Other factors such as presence of divalent ions in the leaching water also showed to have an effect on the hydraulic conductivity with divalent ions increasing the flow rate through setup E and F. The increase in pH of water used for leaching did not show to have an effect on the dissolution of the silica gels.

6. Future Work

The behaviours of silica nanoparticles and silica gels are complex. A number of parameters such as, particle size, pH, temperature, ion types, ion concentrations, particle concentration, and the nature of the silica surface, will all affect the silica sols and gels. An example of the system complexity is the limitations of gel time predictions by equation 18. Future work should focus on mapping the parameters mentioned above. For these more complex methods such a small angle x-ray scattering or neutron scattering might have to be used to be able to see what occurs on an atom-scale at the silica surface. Furthermore, there are still open questions regarding the mechanisms behind the strength build-up in silica gels. An often cited mechanism for strength build-up is the formation of siloxane (Si-O-Si) bonds between aggregated particles through condensation reaction. The number of siloxane bonds is considered to correspond to gel strength. The nature of this reaction and formation of

siloxane bonds remains unknown and the only real evidence for it occurring is that aged gels (a few hours) cannot be broken up into solution again. Such bond formation would require the dislocation of ions present at the silica surface and questions remain whether this is energetically favourable.

7. Acknowledgements

To start with I would like to thank the persons without which this thesis would never have been written; my supervisor **Zareen Abbas** who has helped and guided me throughout my studies and my Co-supervisor **Johan Funehag** who has taught me a lot about applications of silica sol within grouting. My examiner **Jan Pettersson** deserves a call out for all the talks/"utvecklingsamtal" we have had. I would also like to thank all the current and previous members of the electrochemistry research group at Gothenburg University; **Isabelle Simonsson** my office mate and phd colleague - thank you for the good company, **Adriano Gomes** - thank you for making me feel welcome when I started my phd and all the good AWs, **Alberto Visible** - for all the good times and I hope you enjoy your time at Chalmers, **Krzysztof Kolman** - for all the help and patience with teaching me MD, and all the other current and previous research group members/colleagues: **Elisabet Ahlberg, Khalid Elamin, Gert Göransson, Patrik Larses, Alice Kent, Cedrik Wiberg, and Mikael Wallter**. I would also like to thank all the students that have cooperated with me during their thesis or project works throughout the years: **Mark Rambaran, Fixos A. Liverios, Robin Nilsson, Amanda Westerlund, Max Christensson, and Ayşe Birsen Otyakmaz**.

Research engineers **Anders Lennartsson** and **Camilla Forsman** deserves a big thank you for all the help with the teaching labs and for making the teaching bearable.

To my family; **Thorkild Sögaard, Eva Sögaard, and Petra Sögaard**, a big thank you for all the support and encouragement throughout the years and for always showing patience when I talk about my, for most people, tedious and abstract work.

Finally to **Beata Himmelmann** who came into my life about halfway through this phd project and who has brightened the final years of this project with her love, company and support.

8. References

1. Lützenkirchen J, Preočanin T, Kovačević D, Tomišić V, Lövgren L, Kallay N. Potentiometric titrations as a tool for surface charge determination. *Croatica chemica acta*. 2012;85(4):391-417.
2. Whitesides GM. Nanoscience, Nanotechnology, and Chemistry. *Small*. 2005;1(2):172-9.
3. Dickinson E. Food colloids — An overview. *Colloids and Surfaces*. 1989;42(1):191-204.
4. Koepenick M. Papermaking on a nano scale. *PULP & PAPER-CANADA*. 2009;110(6):14-6.
5. Edwards-Jones V. The benefits of silver in hygiene, personal care and healthcare. *Letters in Applied Microbiology*. 2009;49(2):147-52.
6. Das SK, Das AR, Guha AK. Gold Nanoparticles: Microbial Synthesis and Application in Water Hygiene Management. *Langmuir*. 2009;25(14):8192-9.
7. Ertmer C, Rehberg S, Van Aken H, Westphal M. Relevance of non-albumin colloids in intensive care medicine. *Best Practice & Research Clinical Anaesthesiology*. 2009;23(2):193-212.
8. Bergna HE. ACS publications. *Colloid Chemistry of Silica: an Overview*. 1994:43.
9. Funehag J, Fransson Å. Sealing narrow fractures with a Newtonian fluid: Model prediction for grouting verified by field study. *Tunnelling and Underground Space Technology*. 2006;21(5):492-8.
10. Yang Q, Zhao M, Gao M, Song X, Dai C. The experimental study of silica nanoparticles strengthened polymer gel system. *Journal of Dispersion Science and Technology*. 2019:1-8.
11. Miranda CR, Lara LSd, Tonetto BC. Stability and Mobility of Functionalized Silica Nanoparticles for Enhanced Oil Recovery Applications. SPE International Oilfield Nanotechnology Conference and Exhibition; 2012/1/1/; Noordwijk, The Netherlands. SPE: Society of Petroleum Engineers; 2012. p. 11.
12. Tsuji M, Kobayashi S, Mikake S, Sato T, Matsui H. Post-Grouting Experiences for Reducing Groundwater Inflow at 500 m Depth of the Mizunami Underground Research Laboratory, Japan. *Procedia engineering*. 2017;191:543-50.
13. Funehag J, Gustafson G. Design of grouting with silica sol in hard rock – New design criteria tested in the field, Part II. *Tunnelling and Underground Space Technology*. 2008;23(1):9-17.
14. Funehag J, Gustafson G. Design of grouting with silica sol in hard rock – New methods for calculation of penetration length, Part I. *Tunnelling and Underground Space Technology*. 2008;23(1):1-8.
15. Persoff P, Apps J, Moridis G, Whang JM. Effect of dilution and contaminants on sand grouted with colloidal silica. *Journal of Geotechnical and Geoenvironmental Engineering*. 1999;125(6):461-9.
16. Holttä P, Lahtinen M, Hakanen M, Lehto J, Juhola P. The influence of groundwater on the stability of silica colloids. *MRS Online Proceedings Library Archive*. 2009;1193.
17. Karol RH. *Chemical grouting*: Marcel dekker; 1990.
18. *Chemical Grouting* https://www.publications.usace.army.mil/USACE-Publications/Engineer-Manuals/%3fudt_43544_param_page%3d3: HQ US Army Corps of Engineers; 1995 [
19. Funehag J. *Guide to Grouting with Silica Sol: For Sealing in Hard Rock*: Stiftelsen Bergteknisk forskning; 2012.
20. Müller HS, Haist M, Vogel M. Assessment of the sustainability potential of concrete and concrete structures considering their environmental impact, performance and lifetime. *Construction and Building Materials*. 2014;67:321-37.
21. Cademartiri L, Ozin GA. *Concepts of nanochemistry*: John Wiley & Sons; 2009.
22. Berg J. *An introduction to interfaces & colloids: the bridge to nanoscience*. 2010, Hackensack: NJ: World Scientific.

23. Rahman IA, Padavettan V. Synthesis of silica nanoparticles by sol-gel: size-dependent properties, surface modification, and applications in silica-polymer nanocomposites—a review. *Journal of Nanomaterials*. 2012;2012:8.
24. Hench LL, West JK. The sol-gel process. *Chemical reviews*. 1990;90(1):33-72.
25. Stöber W, Fink A, Bohn E. Controlled growth of monodisperse silica spheres in the micron size range. *Journal of colloid and interface science*. 1968;26(1):62-9.
26. Bogush GH, Tracy MA, Zukoski CF. Preparation of monodisperse silica particles: Control of size and mass fraction. *Journal of Non-Crystalline Solids*. 1988;104(1):95-106.
27. Matsoukas T, Gulari E. Dynamics of growth of silica particles from ammonia-catalyzed hydrolysis of tetra-ethyl-orthosilicate. *Journal of Colloid and Interface Science*. 1988;124(1):252-61.
28. Blute I, Pugh RJ, van de Pas J, Callaghan I. Silica nanoparticle sols: 1. Surface chemical characterization and evaluation of the foam generation (foamability). *Journal of colloid and interface science*. 2007;313(2):645-55.
29. Iler RK. *The Chemistry of Silica: Solubility, Polymerization, Colloid and Surface Properties and Biochemistry of Silica*; Wiley; 1979.
30. Hiemstra T, De Wit JCM, Van Riemsdijk WH. Multisite proton adsorption modeling at the solid/solution interface of (hydr)oxides: A new approach: II. Application to various important (hydr)oxides. *Journal of Colloid and Interface Science*. 1989;133(1):105-17.
31. Leroy P, Devau N, Revil A, Bizi M. Influence of surface conductivity on the apparent zeta potential of amorphous silica nanoparticles. *Journal of colloid and interface science*. 2013;410:81-93.
32. Sverjensky DA. Prediction of surface charge on oxides in salt solutions: revisions for 1: 1 (M+ L-) electrolytes. *Geochimica et Cosmochimica Acta*. 2005;69(2):225-57.
33. Sonnefeld J, Löbbus M, Vogelsberger W. Determination of electric double layer parameters for spherical silica particles under application of the triple layer model using surface charge density data and results of electrokinetic sonic amplitude measurements. *Colloids and Surfaces A: Physicochemical and Engineering Aspects*. 2001;195(1-3):215-25.
34. Duval Y, Mielczarski J, Pokrovsky O, Mielczarski E, Ehrhardt J. Evidence of the existence of three types of species at the quartz- aqueous solution interface at pH 0- 10: XPS surface group quantification and surface complexation modeling. *The Journal of Physical Chemistry B*. 2002;106(11):2937-45.
35. Bolt GH. Determination of the Charge Density of Silica Sols. *The Journal of Physical Chemistry*. 1957;61(9):1166-9.
36. Brown MA, Belouqui Redondo A, Sterrer M, Winter B, Pacchioni G, Abbas Z, et al. Measure of surface potential at the aqueous-oxide nanoparticle interface by XPS from a liquid microjet. *Nano letters*. 2013;13(11):5403-7.
37. Allen LH, Matijević E, Meites L. Exchange of Na+ for the silanolic protons of silica. *Journal of Inorganic and Nuclear Chemistry*. 1971;33(5):1293-9.
38. Ong S, Zhao X, Eisenthal KB. Polarization of water molecules at a charged interface: second harmonic studies of the silica/water interface. *Chemical Physics Letters*. 1992;191(3):327-35.
39. Pfeiffer-Laplaud M, Costa D, Tielens F, Gageot M-P, Sulpizi M. Bimodal acidity at the amorphous silica/water interface. *The Journal of Physical Chemistry C*. 2015;119(49):27354-62.
40. Bergström L. Hamaker constants of inorganic materials. *Advances in Colloid and Interface Science*. 1997;70:125-69.
41. Grasso D, Subramaniam K, Butkus M, Strevett K, Bergendahl J. A review of non-DLVO interactions in environmental colloidal systems. *Reviews in Environmental Science and Biotechnology*. 2002;1(1):17-38.
42. Hotze EM, Phenrat T, Lowry GV. Nanoparticle aggregation: challenges to understanding transport and reactivity in the environment. *Journal of environmental quality*. 2010;39(6):1909-24.

43. Phenrat T, Saleh N, Sirk K, Tilton RD, Lowry GV. Aggregation and sedimentation of aqueous nanoscale zerovalent iron dispersions. *Environmental Science & Technology*. 2007;41(1):284-90.
44. Hoek EM, Agarwal GK. Extended DLVO interactions between spherical particles and rough surfaces. *Journal of Colloid and Interface science*. 2006;298(1):50-8.
45. Wu W, Giese R, Van Oss C. Stability versus flocculation of particle suspensions in water—correlation with the extended DLVO approach for aqueous systems, compared with classical DLVO theory. *Colloids and Surfaces B: Biointerfaces*. 1999;14(1-4):47-55.
46. Fritz G, Schädler V, Willenbacher N, Wagner NJ. Electrosteric stabilization of colloidal dispersions. *Langmuir*. 2002;18(16):6381-90.
47. Ortega-Vinuesa J, Martín-Rodríguez A, Hidalgo-Alvarez R. Colloidal stability of polymer colloids with different interfacial properties: mechanisms. *Journal of colloid and interface science*. 1996;184(1):259-67.
48. Phenrat T, Saleh N, Sirk K, Kim H-J, Tilton RD, Lowry GV. Stabilization of aqueous nanoscale zerovalent iron dispersions by anionic polyelectrolytes: adsorbed anionic polyelectrolyte layer properties and their effect on aggregation and sedimentation. *Journal of Nanoparticle Research*. 2008;10(5):795-814.
49. Romero-Cano M, Martín-Rodríguez A, De Las Nieves F. Electrosteric stabilization of polymer colloids with different functionality. *Langmuir*. 2001;17(11):3505-11.
50. Chen KL, Elimelech M. Influence of humic acid on the aggregation kinetics of fullerene (C60) nanoparticles in monovalent and divalent electrolyte solutions. *Journal of colloid and interface science*. 2007;309(1):126-34.
51. Domingos RF, Tufenkji N, Wilkinson KJ. Aggregation of titanium dioxide nanoparticles: role of a fulvic acid. *Environmental Science & Technology*. 2009;43(5):1282-6.
52. Boström M, Deniz V, Franks G, Ninham B. Extended DLVO theory: Electrostatic and non-electrostatic forces in oxide suspensions. *Advances in Colloid and Interface Science*. 2006;123:5-15.
53. Zhang H, Hassanali AA, Shin YK, Knight C, Singer SJ. The water–amorphous silica interface: Analysis of the Stern layer and surface conduction. *The Journal of chemical physics*. 2011;134(2):024705.
54. Travesset A, Vangaveti S. Electrostatic correlations at the Stern layer: Physics or chemistry? *The Journal of chemical physics*. 2009;131(18):11B608.
55. Lyklema J. Simple Hofmeister series. *Chemical Physics Letters*. 2009;467(4-6):217-22.
56. Ninham BW, Yaminsky V. Ion binding and ion specificity: the Hofmeister effect and Onsager and Lifshitz theories. *Langmuir*. 1997;13(7):2097-108.
57. Hofmeister F. Zur lehre von der wirkung der salze. *Archiv für experimentelle Pathologie und Pharmakologie*. 1888;25(1):1-30.
58. Dove PM, Craven CM. Surface charge density on silica in alkali and alkaline earth chloride electrolyte solutions. *Geochimica et Cosmochimica Acta*. 2005;69(21):4963-70.
59. Johnson A-CJ, Greenwood P, Hagström M, Abbas Z, Wall S. Aggregation of nanosized colloidal silica in the presence of various alkali cations investigated by the electrospray technique. *Langmuir*. 2008;24(22):12798-806.
60. Depasse J, Watillon A. The stability of amorphous colloidal silica. *Journal of colloid and interface science*. 1970;33(3):430-8.
61. Marcus Y. Thermodynamics of solvation of ions. Part 5.—Gibbs free energy of hydration at 298.15 K. *Journal of the Chemical Society, Faraday Transactions*. 1991;87(18):2995-9.
62. Abbas Z, Ahlberg E, Nordholm S. Monte Carlo simulations of salt solutions: exploring the validity of primitive models. *The journal of physical chemistry B*. 2009;113(17):5905-16.
63. Buchner R, Hefter G. Interactions and dynamics in electrolyte solutions by dielectric spectroscopy. *Physical Chemistry Chemical Physics*. 2009;11(40):8984-99.
64. Nightingale Jr E. Phenomenological theory of ion solvation. Effective radii of hydrated ions. *The Journal of Physical Chemistry*. 1959;63(9):1381-7.

65. Trompette J, Meireles M. Ion-specific effect on the gelation kinetics of concentrated colloidal silica suspensions. *Journal of colloid and interface science*. 2003;263(2):522-7.
66. Tamar Y, Sasson Y. Examination of the regime controlling sol–gel based colloidal silica aggregation. *Journal of Non-Crystalline Solids*. 2013;380:35-41.
67. Huang J, Al-Mohsin A, Bataweel M, Karadkar P, Li W, Shaikh A, editors. Systematic approach to develop a colloidal silica based gel system for water shut-off. SPE Middle East Oil & Gas Show and Conference; 2017: Society of Petroleum Engineers.
68. Okazaki K, Kawaguchi M. Influence of monovalent electrolytes on rheological properties of gelled colloidal silica suspensions. *Journal of Dispersion Science and Technology*. 2008;29(1):77-82.
69. Dickinson E. Structure and rheology of simulated gels formed from aggregated colloidal particles. *Journal of colloid and interface science*. 2000;225(1):2-15.
70. Jullien R, Botet R. Aggregation and fractal aggregates. *Ann Telecomm*. 1987;41:343 (short version).
71. Bremer LGB, Bijsterbosch BH, Walstra P, van Vliet T. Formation, properties and fractal structure of particle gels. *Advances in Colloid and Interface Science*. 1993;46:117-28.
72. Alexander GB, Heston W, Iler RK. The solubility of amorphous silica in water. *The Journal of Physical Chemistry*. 1954;58(6):453-5.
73. Ågren P, Rosenholm J. Phase behavior and structural changes in tetraethylorthosilicate-derived gels in the presence of polyethylene glycol, studied by rheological techniques and visual observations. *Journal of colloid and interface science*. 1998;204(1):45-52.
74. Mack CA. Fifty Years of Moore's Law. *IEEE Transactions on Semiconductor Manufacturing*. 2011;24(2):202-7.
75. Jenkins S, Kirk SR, Persson M, Carlen J, Abbas Z. Molecular dynamics simulation of nanocolloidal amorphous silica particles: Part II. *The Journal of chemical physics*. 2008;128(16):164711.
76. Kolman K, Abbas Z. Molecular dynamics exploration for the adsorption of benzoic acid derivatives on charged silica surfaces. *Colloids and Surfaces A: Physicochemical and Engineering Aspects*. 2019;578:123635.
77. Van Der Spoel D, Lindahl E, Hess B, Groenhof G, Mark AE, Berendsen HJC. GROMACS: Fast, flexible, and free. *Journal of Computational Chemistry*. 2005;26(16):1701-18.
78. MacKerell AD, Bashford D, Bellott M, Dunbrack RL, Evanseck JD, Field MJ, et al. All-Atom Empirical Potential for Molecular Modeling and Dynamics Studies of Proteins. *The Journal of Physical Chemistry B*. 1998;102(18):3586-616.
79. Jorgensen WL, Chandrasekhar J, Madura JD, Impey RW, Klein ML. Comparison of simple potential functions for simulating liquid water. *The Journal of Chemical Physics*. 1983;79(2):926-35.
80. MALVERN. Zetasizer Nano User Manual: Malvern Instruments Ltd; 2013.
81. Barnes HA, Hutton JF, Walters K. *An introduction to rheology*: Elsevier; 1989.
82. Paar A. Basics of rheology <https://wiki.anton-paar.com/en/basics-of-rheology/#loss-factor-or-damping-factor-tan-g-g>; wiki.anton-paar.com; 2017 [
83. Harris DC. *Quantitative Chemical Analysis*: W. H. Freeman; 2010.
84. Trefalt G, Szilagyí I, Téllez G, Borkovec M. Colloidal Stability in Asymmetric Electrolytes: Modifications of the Schulze–Hardy Rule. *Langmuir*. 2017;33(7):1695-704.
85. Rouster P, Pavlovic M, Szilagyí I. Destabilization of Titania Nanosheet Suspensions by Inorganic Salts: Hofmeister Series and Schulze-Hardy Rule. *The Journal of Physical Chemistry B*. 2017;121(27):6749-58.
86. Trefalt G. Derivation of the inverse Schulze-Hardy rule. *Physical Review E*. 2016;93(3):032612.
87. Simonsson I, Sögaard C, Rambaran M, Abbas Z. The specific co-ion effect on gelling and surface charging of silica nanoparticles: Speculation or reality? *Colloids and Surfaces A: Physicochemical and Engineering Aspects*. 2018;559:334-41.

88. Hamer WJ, Wu YC. Osmotic Coefficients and Mean Activity Coefficients of Uni-univalent Electrolytes in Water at 25°C. *Journal of Physical and Chemical Reference Data*. 1972;1(4):1047-100.
89. Goldberg RN. Evaluated activity and osmotic coefficients for aqueous solutions: thirty-six uni-bivalent electrolytes. *Journal of Physical and Chemical Reference Data*. 1981;10(3):671-764.
90. Wright MR. *An introduction to aqueous electrolyte solutions*: John Wiley & Sons; 2007.
91. DeWalt-Kerian EL, Kim S, Azam MS, Zeng H, Liu Q, Gibbs JM. pH-dependent inversion of Hofmeister trends in the water structure of the electrical double layer. *The journal of physical chemistry letters*. 2017;8(13):2855-61.
92. Collins KD. Why continuum electrostatics theories cannot explain biological structure, polyelectrolytes or ionic strength effects in ion–protein interactions. *Biophysical chemistry*. 2012;167:43-59.
93. Johnsson A-CJ, Camerani MC, Abbas Z. Combined electrospray-scanning mobility particle sizer (ES-SMPS) and time-resolved synchrotron radiation-small-angle X-ray scattering (SR-SAXS) investigation of colloidal silica aggregation. Part II. Influence of aggregation initiator on gel stability. *The Journal of Physical Chemistry B*. 2011;115(31):9547-55.
94. Milonjić SK. A relation between the amounts of sorbed alkali cations and the stability of colloidal silica. *Colloids and surfaces*. 1992;63(1-2):113-9.
95. Wang Y, Wang L, Hampton MA, Nguyen AV. Atomic force microscopy study of forces between a silica sphere and an oxidized silicon wafer in aqueous solutions of NaCl, KCl, and CsCl at concentrations up to saturation. *The Journal of Physical Chemistry C*. 2013;117(5):2113-20.
96. Depasse J. Coagulation of colloidal silica by alkaline cations: Surface dehydration or interparticle bridging? *Journal of Colloid and Interface Science*. 1997;194(1):260-2.
97. Trompette J-L, Clifton M. Influence of ionic specificity on the microstructure and the strength of gelled colloidal silica suspensions. *Journal of colloid and interface science*. 2004;276(2):475-82.
98. ben Jabrallah S, Malloggi F, Belloni L, Girard L, Novikov D, Mocuta C, et al. Electrolytes at interfaces: accessing the first nanometers using X-ray standing waves. *Physical Chemistry Chemical Physics*. 2017;19(1):167-74.
99. Metin CO, Lake LW, Miranda CR, Nguyen QP. Stability of aqueous silica nanoparticle dispersions. *Journal of Nanoparticle Research*. 2011;13(2):839-50.